University of West Bohemia
Faculty of applied sciences
Department of Mechanics

DIPLOMA THESIS

Pilsen 2020

Pavel Halama

University of West Bohemia
Faculty of applied sciences
Department of Mechanics

DIPLOMA THESIS

Modelling and dynamic analysis of rotating systems with nonlinearities

Pilsen 2020

Pavel Halama

Declaration

I hereby certify that this diploma thesis is entirely the result of my work and I faithfully and properly cited all sources used in the thesis.

In Pilsen 30.6.2020

.....
signature

Acknowledgements

I would like to thank my supervisor, Ing. Miroslav Byrtus Ph.D for his support while writing this diploma thesis. I would also like to thank to Ing. Josef Otta Ph.D for his support and provided materials. I have to express my very profound gratitude to my parents and to my girlfriend for providing me with unfailing support and continuous encouragement throughout my years of study and through the process of researching and writing this thesis. This accomplishment would not have been possible without them.

Abstract

This diploma thesis deals with mathematical modelling and dynamic analysis of complex rotating systems connected by nonlinear couplings. These systems can be divided into subsystems like shafts or bearings. We can model these subsystems separately and than connect them using modal synthesis method. In the first part of the thesis, the approach of modelling of these subsystems using finite element method is described. Mathematical models of shafts, journal bearings, gearing are described as well as their interconnection to the whole system. The journal bearing nonlinear forces are obtained via a analytical solution of Reynolds equation for special types of bearings. In the mathematical model of gearing, non-linear effects like backslash can be considered as well as kinematic transmission error as the main source of internal excitation.

In the second part, approaches to the evaluation of dynamic analysis of the rotating systems are mentioned. These approaches include modal analysis, stability analysis or modal synthesis which allow us to reduce number of degrees of freedom of the models.

In the application part of the thesis, three applications of the proposed methods are created. According to the mathematical models, computational models for all three applications were developed in computational system MATLAB. Computational models were used for examination of typical non-linear phenomena in rotating systems.

Abstrakt

Diplomová práce se věnuje matematickému modelování a dynamické analýze komplexních rotujících soustav, které jsou provázány nelineárními vazbami. Tyto systémy mohou být dekomponovány na subsystémy jako hřídele, ložiska nebo ozubení. Tyto subsystémy lze modelovat samostatně a poté pomocí metody modální syntézy propojit v celek. V první části práce jsou uvedeny přístupy k modelování uvedených subsystémů metodou konečných prvků. Hydrodynamické síly v ložiskách jsou získány pomocí analytického řešení Reynoldsovy rovnice pro speciální případy ložisek, tj. krátká nebo dlouhá ložiska. Matematický model ozubení umožňuje simulovat lineární i nelineární jevy, které se ve vnitřní dynamice ozubených převodů vyskytují. Mezi tyto jevy lze zahrnout kinematickou úchylku ozubení, jakožto hlavní zdroj vnitřního buzení, nebo nelineární model vůle v ozubení, který v modelu vytváří silnou nelinearitu.

Druhá část práce se zabývá přístupy k dynamické analýze rotujících systémů a to především převedení matematického modelu do stavového prostoru, modální analýzou, stabilitou a modální syntézou, která pomocí modální redukce počtu stupňů volnosti umožňuje redukované subsystémy propojit v globální matematický model.

V aplikační části práce jsou uvedeny tři aplikace uvedených metod a přístupu k modelování dynamických systémů. Na základě matematických modelů byly vytvořeny výpočtové modely v programovém prostředí MATLAB, které umožňují zkoumat typické nelinární jevy vyskytujících se v kmitajících rotujících soustavách.

Contents

1 Introduction

Dynamic analysis of shafts and gearboxes is still a current topic. Fluid bearings are more and more used for supporting these types of systems. The main reason for their use is low friction and dynamic response caused by hydrodynamic forces [4]. There are many types of fluid bearings. For example, there are bearings with grooves, bearings with tilting segments or bearings with floating rings. Dynamic behaviour of rotors supported by fluid bearings is mainly influenced by stability of the bearings [3]. As the rotor speed increases, instability may occur in the bearing. There are two main types of fluid bearing instability. The instability of type *oil whirl* causes self-excited vibrations of the rotor at roughly 0.42–0.49 of the shaft speed [14]. *Oil whip* occurs when the whirl frequency is close to some of the system natural frequency [14].

Other coupling that has a significant influence on the dynamic behaviour is a gearing. The main impact on the gearbox dynamic response have linear and non-linear effects in the gears including tooth backlash, time-varying mesh stiffness or kinematic transmission error [1]. Backslash describes a gap between mating teeth in the gearing and can cause intermittent loss of contact between the teeth creating a non-linear force. Time-varying meshing stiffness and kinematic transmission error is mainly caused by alternating the number of teeth in the meshing gears and by manufacturing inaccuracies. These phenomena are the main source of internal excitation and may lead to parametric resonances [2].

Modelling and detection of these phenomena is therefore in the interest of many research institutes.

1.1 State of the art

There are many publications that focus on the rotor dynamic in the literature. Detailed description of dynamic behaviour of rotors are summarized for example in [9] or [8]. Dynamic analysis including approach of modal reduction of system of shafts using finite element method is described in [6]. These publications aim at modelling and dynamic analysis of rotors supported by several bearings using both numerical and analytical approach. In [10] and [11], the methodology of modelling of flexible stator is listed.

If it comes to modelling of fluid bearings and its dynamic behaviour, many publications have been recently published. Model of a fluid bearing is connected with the model of rotor by a vector of hydrodynamic forces acting on the specific position of the rotor. There are several approaches that we can use for expressing the hydrodynamic forces. Recently, analytical approaches have been used for expressing hydrodynamic forces in fluid bearings. Analytical approach for specific types of fluid bearings is described for example in [5] or [13]. Numerical approaches using finite diffference, finite element or finite volume method are summarized in [16], [17] or [18]. There are many publications that deal with dynamic analysis of rotors supported by fluid bearings. For example, dynamics of the rotor-fluid bearing system is described in [5] or [12]. In [13], it has been proved that the dynamic behaviour of rotor depends on the stability of the fluid bearing. The publication [14] studied the dynamic behaviour of fluid bearings with 2 oil films and it has been shown that the instability can be suppressed by using this type of fluid bearing, especially for high-speed turbochargers.

Many publications have also studied dynamic behaviour of gearing. Recently in the 1990s, publications like [19] analyzed the effect of backlash on a single-degree-of-freedom gear model using both analytical and numerical approach. Article [20] studied non-linear effects in gearing with parametric excitation. Publication [21] experimentally observed chaotic vibration, jump phenomena, and subharmonic response due to parametric and backlash excitations. Nowadays many publications that deals with investigating non-linear phenomena in gearing are beeing created. Article [22] examine the bifurcation characteristics of a three-degree-of-freedom geared rotor-bearing model. Article [27] studied non-linear dynamics of gear-pair systems with periodic stiffness and backlash. Publication [23] performed parametric studies to investigate the influence of the contact ratio, spacing error, transmitted load and mesh damping of a gear. Nonlinear vibration in different types of gears has been investigated and publications have been made, e.g. [24],[25] or [26].

Dynamic analysis of a rotor-gearing system supported by fluid bearings is a current topic and many publications are being developed. This is proved, for example, by publication [28] where the effect of gear and journal bearing parameters on bifurcation, chaos and oil whirl was investigated. Publication [29] showed that a linearized bearing coefficient model does not provide accurate predictions of gear vibrations, especially at high speed and load conditions. Article [30] used the approximate short journal bearing theory and showed that varying the operating speed or applied torque may cause the occurrence of oil whirl response of the rotordynamic systems. One of the latest publication that deals with dynamic analysis of gearboxes supported by fluid bearings is [31], where the non-linear behaviour and bifurcation of a geared rotor system supported by fluid film journal bearings were investigated. During the simulations, it was showed that the input torque and bearing L/D ratio have impact on non-linear gearing phenomenon, especially jump-up and jump-down phenomenon. It was also shown that small bearing L/D ratio, lubricant viscosity and bearing clearance suppress the subharmonic resonances that occurs with parametric excitation. Chaotic motion and bifurcation phenomenon was also studied. The results showed that the high-applied input torques to the gear suppress the chaotic response in the system.

1.2 Thesis goals

The main goals of this thesis can be summarized as:

- Summary the state of the art.
- Mathematical modelling of the gearing with non-linear effects.
- Mathematical modelling of the fluid bearings and flexible shafts.
- Mathematical models of rotating systems.
- Approaches to dynamic analysis of rotating systems.
- Application of proposed methods on specific system.

2 Mathematical modelling of rotating systems

Most of the machinery machines consist of some rotating system, which transmit torgue or mechanical energy through the system. We can divide this system into subsystems like shafts, gears or gearboxes. We can describe these subsystems by creating mathematical models and then we can connect them via bindings. This connection can be done by using modal synthesis method [6]. The next chapter aims at building mathematical models of subsystems that have been mentioned using *finite element method* (FEM).

2.1 Mathematical model of shaft

Shafts belong to fundamental components of rotating systems. Their longitudinal dimension is larger than the transverse and thus it can be considered a transversely incompressible continuum [2]. Let us divide the shaft of circular cross section into the system of shaft elements with the finite number of nodes. The shaft element e of length l, which is placed between nodes A_0 and B_0 (generally "i" and "$i+1$"), is depict in fig. 1. For next derivation let us consider these assumptions [2]:

1. The element rotates with constant angular velocity ω_0 along the longitudinal axes.
2. According to the *Mindlin theory* the cross sections of the shaft stay planar.
3. According to the *Rayleigh theory* the bevel is neglected.
4. Mathematical models are build in fixed space (x,y,z).

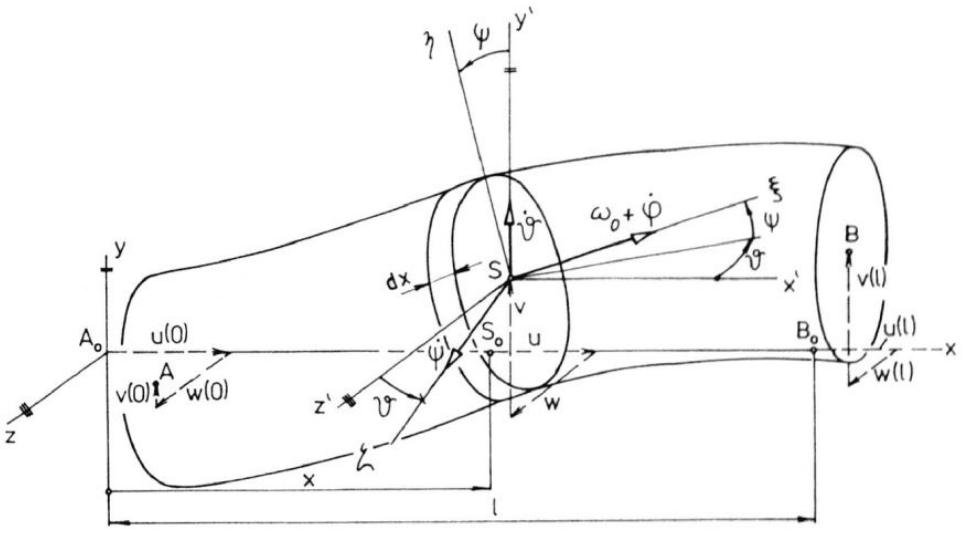

Fig. 1: Shaft element [6]

Matrices of shaft element

The following derivation is taken from [6]. The deformation of the shaft is described in the centre of gravity S by a longitudinal displacement $u(x,t)$, transversal displacements

$v(x,t)$, $w(x,t)$ and by angular displacements of all axes $\varphi(x,t)$, $\theta(x,t)$ a $\psi(x,t)$. According to the considered assumptions we can express kinetic energy E_k^e and potential energy E_p^e of the shaft element which directly depend on the mentioned displacements. We can describe these displacements by using approximation functions. Longitudinal and torsional deformations are approximated by linear polynomials, transverse deformations are approximated by cubic polynomials. Let us implement a vector of the general coordinates of the element shaft in the local coordinate space by displacements of nodes

$$\mathbf{q}^{(e)} = [v(0), \psi(0), v(l), \psi(l), w(0), \vartheta(0), w(l), \vartheta(l), u(0), u(l), \varphi(0), \varphi(l)]^T. \tag{2.1.1}$$

We can then use Lagrange equation of second kind to build matrices of the shaft element $\mathbf{M}^{(e)}$, $\mathbf{G}^{(e)}$ and $\mathbf{K}^{(e)}$, i.e. mass, gyroscopic and stiffness matrix. A detailed derivation of individual matrices can be found in [2] or [6].

The matrices are in this form

$$\begin{aligned}
\mathbf{M}^{(e)} &= \begin{bmatrix} \mathbf{S}_1^{-T}(\mathbf{I}_1+\mathbf{I}_2)\mathbf{S}_1^{-1} & \mathbf{0} & \mathbf{0} & \mathbf{0} \\ \mathbf{0} & \mathbf{S}_2^{-T}(\mathbf{I}_1+\mathbf{I}_2)\mathbf{S}_2^{-1} & \mathbf{0} & \mathbf{0} \\ \mathbf{0} & \mathbf{0} & \mathbf{S}_3^{-T}\mathbf{I}_4\mathbf{S}_3^{-1} & \mathbf{0} \\ \mathbf{0} & \mathbf{0} & \mathbf{0} & \mathbf{S}_3^{-T}\mathbf{I}_5\mathbf{S}_3^{-1} \end{bmatrix}, \\
\mathbf{G}^{(e)} &= \begin{bmatrix} \mathbf{0} & 2\mathbf{S}_1^{-T}\mathbf{I}_2\mathbf{S}_2^{-1} & \mathbf{0} & \mathbf{0} \\ -2\mathbf{S}_2^{-T}\mathbf{I}_2\mathbf{S}_1^{-1} & \mathbf{0} & \mathbf{0} & \mathbf{0} \\ \mathbf{0} & \mathbf{0} & \mathbf{0} & \mathbf{0} \\ \mathbf{0} & \mathbf{0} & \mathbf{0} & \mathbf{0} \end{bmatrix}, \\
\mathbf{K}^{(e)} &= \begin{bmatrix} \mathbf{S}_1^{-T}\mathbf{I}_3\mathbf{S}_1^{-1} & \mathbf{0} & \mathbf{0} & \mathbf{0} \\ \mathbf{0} & \mathbf{S}_2^{-T}\mathbf{I}_3\mathbf{S}_2^{-1} & \mathbf{0} & \mathbf{0} \\ \mathbf{0} & \mathbf{0} & \mathbf{S}_3^{-T}\mathbf{I}_6\mathbf{S}_3^{-1} & \mathbf{0} \\ \mathbf{0} & \mathbf{0} & \mathbf{0} & \mathbf{S}_3^{-T}\mathbf{I}_7\mathbf{S}_3^{-1} \end{bmatrix},
\end{aligned} \tag{2.1.2}$$

In equations (2.1.2), we used approximation matrices

$$\mathbf{S}_1 = \begin{bmatrix} 1 & 0 & 0 & 0 \\ 0 & 1 & 0 & 0 \\ 1 & l & l^2 & l^3 \\ 0 & 1 & 2l & 3l^2 \end{bmatrix}, \quad \mathbf{S}_2 = \begin{bmatrix} 1 & 0 & 0 & 0 \\ 0 & -1 & 0 & 0 \\ 1 & l & l^2 & l^3 \\ 0 & -1 & -2l & -3l^2 \end{bmatrix}, \quad \mathbf{S}_3 = \begin{bmatrix} 1 & 0 \\ 1 & l \end{bmatrix}, \tag{2.1.3}$$

and integral matrices in form

$$
\begin{aligned}
\mathbf{I}_1 &= \rho A l \begin{bmatrix} 1 & l/2 & l^2/3 & l^3/4 \\ & l^2/3 & l^3/4 & l^4/5 \\ & & l^4/5 & l^5/6 \\ & \text{sym.} & & l^6/7 \end{bmatrix}, \quad \mathbf{I}_2 = \rho J l \begin{bmatrix} 0 & 0 & 0 & 0 \\ & 1 & l & l^2 \\ & & 4l^2/3 & 3l^3/2 \\ & \text{sym.} & & 9l^4/5 \end{bmatrix}, \\
\mathbf{I}_3 &= EJl \begin{bmatrix} 0 & 0 & 0 & 0 \\ & 0 & 0 & 0 \\ & & 4 & 6l \\ & \text{sym.} & & 12l^2 \end{bmatrix}, \quad \mathbf{I}_4 = \rho A l \begin{bmatrix} 1 & l/2 \\ l/2 & l^2/3 \end{bmatrix}, \\
\mathbf{I}_5 &= \rho J_p l \begin{bmatrix} 1 & l/2 \\ l/2 & l^2/3 \end{bmatrix}, \quad \mathbf{I}_6 = EAl \begin{bmatrix} 0 & 0 \\ 0 & 1 \end{bmatrix}, \quad \mathbf{I}_6 = GJ_p l \begin{bmatrix} 0 & 0 \\ 0 & 1 \end{bmatrix},
\end{aligned} \tag{2.1.4}
$$

where ρ is density, A is cross section area, J is the second moment of area, E is Young's modulus, J_p is polar moment of area and G is modulus of rigidity of shaft element.

Simplified matrices of shaft element

According to the *Bernoulli-Euler theory* we can neglect the bevel and kinetic energy of the element in the $\xi\eta$ and $\xi\zeta$ plane, the matrices (2.1.2) can be than simplified to the form [6]

$$
\begin{aligned}
\mathbf{M}^{(e)} &= \begin{bmatrix} \mathbf{S}_1^{-T}\mathbf{I}_1\mathbf{S}_1^{-1} & \mathbf{0} & \mathbf{0} & \mathbf{0} \\ \mathbf{0} & \mathbf{S}_2^{-T}\mathbf{I}_1\mathbf{S}_2^{-1} & \mathbf{0} & \mathbf{0} \\ \mathbf{0} & \mathbf{0} & \mathbf{S}_3^{-T}\mathbf{I}_4\mathbf{S}_3^{-1} & \mathbf{0} \\ \mathbf{0} & \mathbf{0} & \mathbf{0} & \mathbf{S}_3^{-T}\mathbf{I}_5\mathbf{S}_3^{-1} \end{bmatrix}, \\
\mathbf{G}^{(e)} &= \begin{bmatrix} \mathbf{0} & 2\mathbf{S}_1^{-T}\mathbf{I}_2\mathbf{S}_2^{-1} & \mathbf{0} & \mathbf{0} \\ -2\mathbf{S}_2^{-T}\mathbf{I}_2\mathbf{S}_1^{-1} & \mathbf{0} & \mathbf{0} & \mathbf{0} \\ \mathbf{0} & \mathbf{0} & \mathbf{0} & \mathbf{0} \\ \mathbf{0} & \mathbf{0} & \mathbf{0} & \mathbf{0} \end{bmatrix}, \\
\mathbf{K}^{(e)} &= \begin{bmatrix} \mathbf{S}_1^{-T}\mathbf{I}_3\mathbf{S}_1^{-1} & \mathbf{0} & \mathbf{0} & \mathbf{0} \\ \mathbf{0} & \mathbf{S}_2^{-T}\mathbf{I}_3\mathbf{S}_2^{-1} & \mathbf{0} & \mathbf{0} \\ \mathbf{0} & \mathbf{0} & \mathbf{S}_3^{-T}\mathbf{I}_6\mathbf{S}_3^{-1} & \mathbf{0} \\ \mathbf{0} & \mathbf{0} & \mathbf{0} & \mathbf{S}_3^{-T}\mathbf{I}_7\mathbf{S}_3^{-1} \end{bmatrix},
\end{aligned} \tag{2.1.5}
$$

Mathematical model of whole shaft

Let us suppose an isolated shaft which we can divide into elements with m nodes, the whole system consist of $m-1$ elements. To create the mathematical model of the whole shaft, it is convenient to transform the matrices (2.1.2) to the different configuration space [2] in form

$$
\mathbf{q}_e = [u(0), v(0), w(0), \varphi(0), \vartheta(0), \psi(0), u(l), v(l), w(l), \varphi(l), \vartheta(l), \psi(l)]^T. \tag{2.1.6}
$$

The relationship between the original space (2.1.1) and the new configuration space (2.1.6) is

$$\mathbf{q}^{(e)} = \mathbf{P}\mathbf{q}_e, \tag{2.1.7}$$

where $\mathbf{P}$ is a permutation matrix, which can be express as

$$\mathbf{P} = \begin{bmatrix} 0 & 1 & 0 & 0 & 0 & 0 & 0 & 0 & 0 & 0 & 0 & 0 \\ 0 & 0 & 0 & 0 & 0 & 1 & 0 & 0 & 0 & 0 & 0 & 0 \\ 0 & 0 & 0 & 0 & 0 & 0 & 0 & 1 & 0 & 0 & 0 & 0 \\ 0 & 0 & 0 & 0 & 0 & 0 & 0 & 0 & 0 & 0 & 0 & 1 \\ 0 & 0 & 1 & 0 & 0 & 0 & 0 & 0 & 0 & 0 & 0 & 0 \\ 0 & 0 & 0 & 0 & 1 & 0 & 0 & 0 & 0 & 0 & 0 & 0 \\ 0 & 0 & 0 & 0 & 0 & 0 & 0 & 0 & 1 & 0 & 0 & 0 \\ 0 & 0 & 0 & 0 & 0 & 0 & 0 & 0 & 0 & 0 & 1 & 0 \\ 1 & 0 & 0 & 0 & 0 & 0 & 0 & 0 & 0 & 0 & 0 & 0 \\ 0 & 0 & 0 & 0 & 0 & 0 & 1 & 0 & 0 & 0 & 0 & 0 \\ 0 & 0 & 0 & 1 & 0 & 0 & 0 & 0 & 0 & 0 & 0 & 0 \\ 0 & 0 & 0 & 0 & 0 & 0 & 0 & 0 & 0 & 1 & 0 & 0 \end{bmatrix}. \tag{2.1.8}$$

We can then transform the matrices (2.1.1) or (2.1.6) to the new configuration space by

$$\mathbf{X}_e = \mathbf{P}^T\mathbf{X}^{(e)}\mathbf{P}, \quad \mathbf{X} = \mathbf{M}, \mathbf{G}, \mathbf{K}. \tag{2.1.9}$$

If we create an array of global coordinates

$$\mathbf{q}(t) = [..., u_i, v_i, w_i, \varphi_i, \vartheta_i, \psi_i...]^T \in \mathbb{R}^n, \tag{2.1.10}$$

where $n = 6m$ is the total degree of freedom, we can then build a mathematical model of isolated undamped shaft in form [2]

$$\mathbf{M}\ddot{\mathbf{q}}(t) + \omega_0\mathbf{G}\dot{\mathbf{q}}(t) + \mathbf{K}\mathbf{q}(t) = \mathbf{0}. \tag{2.1.11}$$

Where global matrix of mass, stiffness and gyroscopic effects are according to the coordinates (2.1.6) and (2.1.10) build of transformed matrices (2.1.2) or (2.1.5) by the scheme in fig.2, where $\mathbf{q}_i$ corresponds to the coordinates of the ith node and $\mathbf{q}_e$ corresponds to the coordinates of the specific element.

Each of the block matrix (highlighted square) is order of 12 and corresponds to the specific shaft element described in transformed coordinate space. This scheme is applied to all matrices.

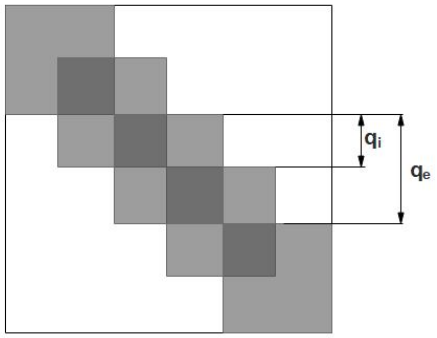

Fig. 2: Scheme of ordering transformed matrices of shaft element in global matrix

2.2 Mathematical model of disc

The following derivation is also taken from [6]. Let us consider a symmetrical rigid disc with a centre of gravity S which is eccentrically mounted on shaft in node i. The scheme of mounting the disk on shaft is depict on fig. 3.

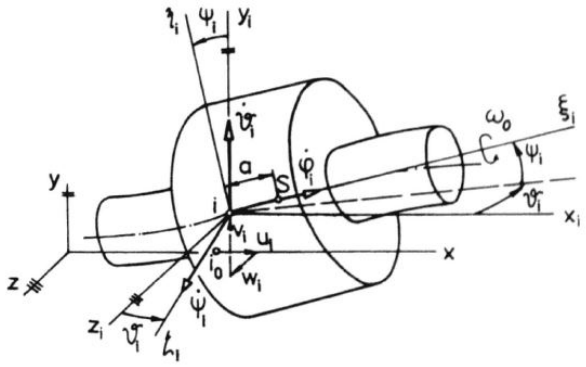

Fig. 3: Scheme of rotating disc [6]

Disc is characterized by the mass m and matrix of inertia $\mathbf{I} = \text{diag}(I_0, I, I)$ where I_0 is a moment of inertia along the longitudinal axes and I is the moment of inertia along both transversal axes. Let us consider these assumptions:

1. Small anglular displacements.
2. Small relative velocity.
3. Disc is fixed to the shaft.

The derivation is deeply described in [6]. If we create an vector of generalized coordinates of the disc in i-node

$$\mathbf{q}_i^{(k)} = [u_i, v_i, w_i, \varphi_i, \vartheta_i, \psi_i]^T, \tag{2.2.1}$$

we can then create a kinetic energy and build a mathematical model of the disc using Lagrange equation of second kind. The matrices of mass and gyrospcopic effect of the disc are in form

$$\mathbf{M}^{(k)} = \begin{bmatrix} m & 0 & 0 & 0 & 0 & 0 \\ & m & 0 & 0 & 0 & ma \\ & & m & 0 & -ma & 0 \\ & & & I_0 & 0 & 0 \\ & & & & I + ma^2 & 0 \\ & sym. & & & & I + ma^2 \end{bmatrix}, \quad \mathbf{G}^{(k)} = \begin{bmatrix} 0 & 0 & 0 & 0 & 0 & 0 \\ 0 & 0 & 0 & 0 & 0 & 0 \\ 0 & 0 & 0 & 0 & 0 & 0 \\ 0 & 0 & 0 & 0 & 0 & 0 \\ 0 & 0 & 0 & 0 & 0 & I_0 \\ 0 & 0 & 0 & 0 & -I_0 & 0 \end{bmatrix}. \tag{2.2.2}$$

We can then put these matrices to the global model of shaft (2.1.11) by scheme depict in fig. 4 where $\mathbf{X} = \mathbf{M}, \mathbf{G}$.

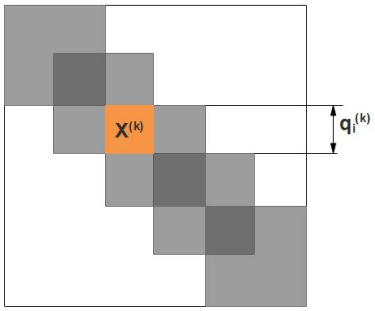

Fig. 4: Scheme of placing disc matrices to global system

2.3 Mathematical model of fluid bearings

The theory of this chapter is inspired by [5] and [4]. Journal bearings are being used in the field of rotating systems because they can provide a sufficient support of high-speed rotating shafts. Between a rotating shaft and non-rotating bearing shell is usually a viscous lubricant. Relative motion of journal and the shell surfaces are essential conditions for the occurrence of hydrodynamic pressure in the lubricant. The hydrodynamic pressure phenomenon creates hydrodynamic forces which are applied to both the shaft and bearing shell. Stable trajectories of the shaft are located close to its static equilibrium position, which is determined by the weight of the supported rotor and by external loads include the hydrodynamic forces. The concept of the separation of the shaft's and shell's surfaces by a thin viscous film with the load carrying ability is known as hydrodynamic lubrication [5].

Hydrodynamic forces

To express hydrodynamic forces, it is convenient to describe the displacement of the shaft by dimensionless eccentricity $\varepsilon(t) = e(t)/c$, where $e(t)$ is an actual eccentricity of the journal center and c is radial clearance of the bearing, and angle $\Phi(t)$ determines the angular position of the journal centre. According to the fig. 5 we can express these variables in this form [5]

$$\varepsilon(t) = \frac{1}{c}\sqrt{x(t)^2 + y(t)^2}, \quad \Phi(t) = \operatorname{atan2}\left(y(t), x(t)\right), \tag{2.3.1}$$

where $x(t)$ and $y(t)$ are the displacements in the centre of the shaft and $atan2$ is a function defined as

$$\operatorname{atan2}(y,x) = \begin{cases} \arctan(\frac{y}{x}) & \text{if } x > 0, \\ \arctan(\frac{y}{x}) + \pi & \text{if } x < 0 \text{ and } y \geq 0, \\ \arctan(\frac{y}{x}) - \pi & \text{if } x < 0 \text{ and } y < 0, \\ +\frac{\pi}{2} & \text{if } x = 0 \text{ and } y > 0, \\ -\frac{\pi}{2} & \text{if } x = 0 \text{ and } y < 0, \\ \text{undefined} & \text{if } x = 0 \text{ and } y = 0. \end{cases}$$

.

Considering a thin oil-film, hydrodynamic pressure $p = p(z, \theta)$ generated in the oil film bearings can be described by the Reynolds equation [5]

$$\frac{1}{R^2}\frac{\partial}{\partial \Theta}\left(h^3\frac{\partial p}{\partial \Theta}\right) + \frac{\partial}{\partial z}\left(h^3\frac{\partial p}{\partial z}\right) = 6\mu\omega\frac{\partial h}{\partial \Theta} + 12\mu\frac{\partial h}{\partial t}, \tag{2.3.2}$$

where R is the rotor radius, Θ is the angle from a reference direction, h is height of thin oil-film, z is the axial coordinate, ω is the angular velocity and μ is a dynamic viscosity. This equation can be applied to a general bearing, but for infinitely long and infinitely short approximations of the journal bearing, the equation (2.3.2) is reduced so it can be solved analytically. The infinite long approximation solution is based on the assumption that $L/D \to \infty$ and the infinity short solution assumes $L/D \to 0$ [5]. In this work, we will continue to devote these special cases only.

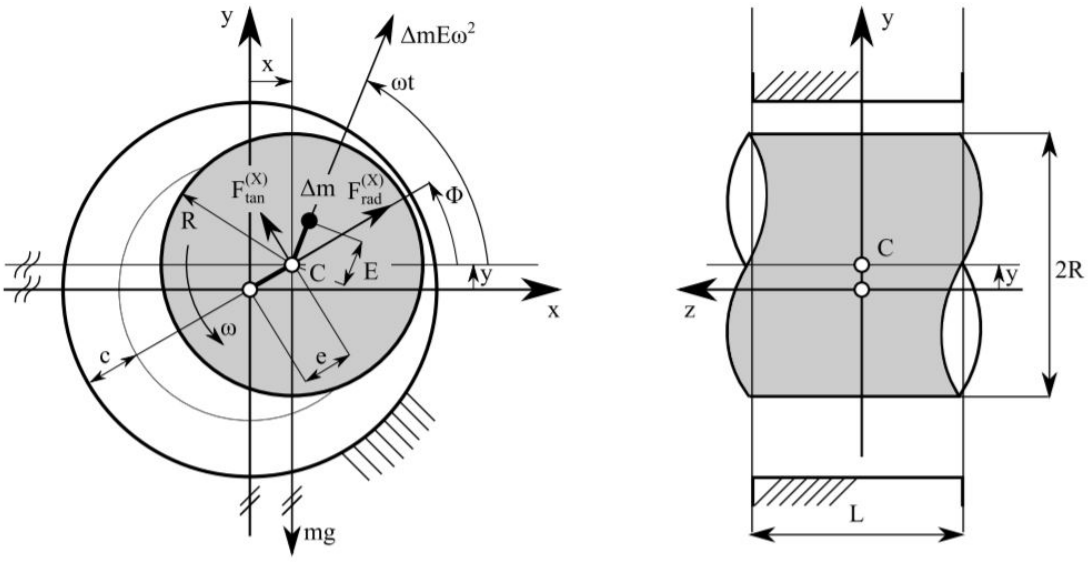

Fig. 5: Scheme of journal bearing [3]

Based on the knowledge of the solution of Reynolds equation (2.3.2), we can then describe the hydrodynamic forces expressed in rotating coordinates in this form

a) Short bearing

$$F_{H,rad} = -\mu RL \left(\frac{L}{c}\right)^2 \left[\left|\omega - 2\dot{\Phi}\right| \frac{\varepsilon^2}{(1-\varepsilon^2)^2} + \frac{\pi(1+2\varepsilon^2)\dot{\varepsilon}}{2(1-\varepsilon^2)^{5/2}}\right], \tag{2.3.3}$$

$$F_{H,tan} = \mu RL \left(\frac{L}{c}\right)^2 \left[(\omega - 2\dot{\Phi}) \frac{\pi\varepsilon}{4(1-\varepsilon^2)^{3/2}} + \frac{2\varepsilon\dot{\varepsilon}}{(1-\varepsilon^2)^2}\right]. \tag{2.3.4}$$

b) Long bearing

$$F_{H,rad} = -6\mu RL \left(\frac{R}{c}\right)^2 \left[\left|\omega - 2\dot{\Phi}\right| \frac{2\varepsilon^2}{(2+\varepsilon^2)(1-\varepsilon^2)} + \frac{\pi\dot{\varepsilon}}{(1-\varepsilon^2)^{3/2}}\right], \tag{2.3.5}$$

$$F_{H,tan} = 6\mu RL \left(\frac{R}{c}\right)^2 \left[(\omega - 2\dot{\Phi}) \frac{\pi\varepsilon}{(2+\varepsilon^2)(1-\varepsilon^2)^{1/2}} + \frac{4\dot{\varepsilon}}{(1+\varepsilon)(1-\varepsilon^2)}\right]. \tag{2.3.6}$$

However, the hydrodynamic forces are formulated in polar coordinates, it is useful to expressed them in fixed space (x,y) using following transformation

$$\begin{bmatrix} F_{H,x} \\ F_{H,y} \end{bmatrix} = \begin{bmatrix} \cos\Phi & -\sin\Phi \\ \sin\Phi & \cos\Phi \end{bmatrix} \begin{bmatrix} F_{H,rad} \\ F_{H,tan} \end{bmatrix}. \tag{2.3.7}$$

Mathematical model of rotor with journal bearings

Let us consider a mathematical model of shaft in the form of (2.1.11) with n-degree of freedom. The vector of generalized has following form [3]

$$\mathbf{q}(t) = [\ldots, u_i, v_i, w_i, \varphi_i, \vartheta_i, \psi_i, \ldots]^T \in \mathbb{R}^n. \tag{2.3.8}$$

where highlighted displacements belong to the deformations of i-node. If we want to put a journal bearing into the i-node with respect to the directions of these deformations in fig. 1, we can form a vector of the hydrodynamic forces on the right side of the global model, which can be expressed as

$$\mathbf{f}_H(\mathbf{q}, \dot{\mathbf{q}}, t) = \begin{bmatrix} \vdots \\ 0 \\ F_{H,y}^{(i)} \\ F_{H,x}^{(i)} \\ 0 \\ 0 \\ 0 \\ \vdots \end{bmatrix} \in \mathbb{R}^n, \tag{2.3.9}$$

The global mathematical model of the rotor with journal bearings can be then expressed as

$$\mathbf{M}\ddot{\mathbf{q}}(t) + \omega_0 \mathbf{G}\dot{\mathbf{q}}(t) + \mathbf{K}\mathbf{q}(t) = \mathbf{f}_H(\mathbf{q}, \dot{\mathbf{q}}, t) + \mathbf{f}_G, \tag{2.3.10}$$

where $\mathbf{f}_G$ is an vector of gravity forces. This system of non-linear differential equations can be solved numerically.

Determination of static equilibrium positions

The static equilibrium is characterized by the presence of static forces only. This means that in (2.3.10), inertial forces $\mathbf{M}\ddot{\mathbf{q}}(t) = \mathbf{0}$, gyroscopic effects $\mathbf{G}\dot{\mathbf{q}}(t) = \mathbf{0}$ and time-variant variables $\dot{\varepsilon} = 0$, $\dot{\Phi} = 0$. The static equilibrium positions represented by an array $\mathbf{q}_R$ can be than calculated using system of non-linear equations

$$\mathbf{K}\mathbf{q}_R = \mathbf{f}_H(\mathbf{q}_R) + \mathbf{f}_G. \tag{2.3.11}$$

Linearization of the hydrodynamic forces

The linearization is based on approximation of the hydrodynamic forces (2.3.7) by the Taylor series in the static equilibrium. Considering only the terms of the first order approximation it can be expressed as

$$F_{H,x} = \underbrace{\left.\frac{\partial F_x}{\partial x}\right|_{\dot{\varepsilon},\dot{\Phi}=0}}_{-k_{xx}} x + \underbrace{\left.\frac{\partial F_x}{\partial y}\right|_{\dot{\varepsilon},\dot{\Phi}=0}}_{-k_{xy}} y + \underbrace{\left.\frac{\partial F_x}{\partial \dot{x}}\right|_{\dot{\varepsilon},\dot{\Phi}=0}}_{-b_{xx}} \dot{x} + \underbrace{\left.\frac{\partial F_x}{\partial \dot{y}}\right|_{\dot{\varepsilon},\dot{\Phi}=0}}_{-b_{xy}} \dot{y}, \tag{2.3.12}$$

$$F_{H,y} = \underbrace{\left.\frac{\partial F_y}{\partial x}\right|_{\dot{\varepsilon},\dot{\Phi}=0}}_{-k_{yx}} x + \underbrace{\left.\frac{\partial F_y}{\partial y}\right|_{\dot{\varepsilon},\dot{\Phi}=0}}_{-k_{yy}} y + \underbrace{\left.\frac{\partial F_y}{\partial \dot{x}}\right|_{\dot{\varepsilon},\dot{\Phi}=0}}_{-b_{yx}} \dot{x} + \underbrace{\left.\frac{\partial F_y}{\partial \dot{y}}\right|_{\dot{\varepsilon},\dot{\Phi}=0}}_{-b_{yy}} \dot{y}. \tag{2.3.13}$$

During the real application, we can use an analytical approach [3]. In the first step, the static equilibrium (2.3.11) is calculated. In the second step, the centre of the shaft is moved by a small distance Δ_j from the static equilibrium position in both directions x and y and it leads to the change of the hydrodynamic forces $\Delta F_{H,i}$. Then the stiffness coefficients are expressed as [3]

$$k_{ij} = -\frac{\Delta F_{H,i}}{\Delta_j}, \quad i,j = x,y. \tag{2.3.14}$$

The damping coefficients are calculated similarly. We can then with respect to the vectr of hydrodynamic forces (2.3.9) create a stiffness and damping matrix of the journal bearings in form [3]

$$\mathbf{K}_b = \begin{bmatrix} & \vdots & \vdots & \\ \dots & k_{xx}^{(i)} & -k_{xy}^{(i)} & \dots \\ \dots & -k_{yx}^{(i)} & k_{yy}^{(i)} & \dots \\ & \vdots & \vdots & \end{bmatrix} \qquad \mathbf{B}_b = \begin{bmatrix} & \vdots & \vdots & \\ \dots & b_{xx}^{(i)} & -b_{xy}^{(i)} & \dots \\ \dots & -b_{yx}^{(i)} & b_{yy}^{(i)} & \dots \\ & \vdots & \vdots & \end{bmatrix}, \tag{2.3.15}$$

and create a complete linearized mathematical model of rotor with journal bearings expressed as

$$\mathbf{M}\ddot{\mathbf{q}}(t) + \omega_0 \left(\mathbf{G} + \mathbf{B}_b\right) \dot{\mathbf{q}}(t) + \left(\mathbf{K} + \mathbf{K}_b\right) \mathbf{q}(t) = \mathbf{0}. \tag{2.3.16}$$

2.4 Mathematical model of gearing

The model created here is inspired by [6], [2] and [7]. Let us suppose a few simplifications when modelling a gear contact. The gear contact is considered to be a point-contact in the center of the tooth thickness, which is linked on the gear mesh line (fig. 6). This simplification can be done for relatively narrow gears. In [2], there is a derivation of gearing deformation between i-node and j-node in the global system, which can be expressed as [6]

$$d_z = \boldsymbol{\delta}_i^T \mathbf{q}_i - \boldsymbol{\delta}_j^T \mathbf{q}_j + \Delta_z(t), \tag{2.4.1}$$

where $\Delta_z(t)$ is a kinematic transmission error and vectors $\boldsymbol{\delta}_i$ and $\boldsymbol{\delta}_j$ can be expressed as [6]

$$\boldsymbol{\delta}_i = \begin{bmatrix} \mp\cos\alpha\sin\beta \\ \sin\alpha\sin\gamma \pm \cos\alpha\cos\beta\cos\gamma \\ -\sin\alpha\cos\gamma \pm \cos\alpha\cos\beta\sin\gamma \\ \pm r_i\cos\alpha\cos\beta \\ \pm r_i\cos\alpha\sin\beta\cos\gamma + a(\sin\alpha\cos\gamma \mp \cos\alpha\cos\beta\sin\gamma) \\ \pm r_i\cos\alpha\sin\beta\sin\gamma + a(\sin\alpha\sin\gamma \pm \cos\alpha\cos\beta\cos\gamma) \end{bmatrix}, \tag{2.4.2}$$

$$\boldsymbol{\delta}_j = \begin{bmatrix} \mp\cos\alpha\sin\beta \\ \sin\alpha\sin\gamma \pm \cos\alpha\cos\beta\cos\gamma \\ -\sin\alpha\cos\gamma \pm \cos\alpha\cos\beta\sin\gamma \\ \mp r_j\cos\alpha\cos\beta \\ \mp r_j\cos\alpha\sin\beta\cos\gamma + a(\sin\alpha\cos\gamma \mp \cos\alpha\cos\beta\sin\gamma) \\ \mp r_j\cos\alpha\sin\beta\sin\gamma + a(\sin\alpha\sin\gamma \pm \cos\alpha\cos\beta\cos\gamma) \end{bmatrix}. \tag{2.4.3}$$

The plus and minus signs are changing according to the way of the shaft rotation. In case of the fig. 6 the upper symbols are applied. See the gearing model in the fig. 6. There are two shafts connected via gearing rotating with constant velocities ω_a and ω_b. Angle α is a pressure angle, β is tooth angle, γ is the deflection angle of the line the center of the rotating discs from the $\hat{xz}$ plane, a and b are distances of centers of the discs and nodes, where the wheels are connected, and r_i, r_j are radii of these wheels. More details can be found in [2].

According to the knowledge of gear deformation (2.4.1), we can then create a potential energy and build a stiffness matrix of the gearing using Lagrange equation of the second kind. The stiffness matrix can be written in this form [6]

$$\mathbf{K}_G^z = k_z\mathbf{C}_z, \qquad \mathbf{C}_z = \begin{bmatrix} & \vdots & \vdots & \\ \dots & \boldsymbol{\delta}_i\boldsymbol{\delta}_j^T & -\boldsymbol{\delta}_i\boldsymbol{\delta}_j^T & \dots \\ & \vdots & \vdots & \\ \dots & -\boldsymbol{\delta}_j\boldsymbol{\delta}_i^T & \boldsymbol{\delta}_j\boldsymbol{\delta}_j^T & \dots \\ & \vdots & \vdots & \end{bmatrix} \in \mathbb{R}^{n,n}, \tag{2.4.4}$$

where k_z is the stiffness of the gearing and n is the degree of freedom of whole system with both shafts. If we want to add to the system damping of the gearing, we can do it by expressing the damping matrix of gearing

$$\mathbf{B}_G^z = b_z\mathbf{C}_z, \tag{2.4.5}$$

where b_z is the damping coefficient of the gearing.

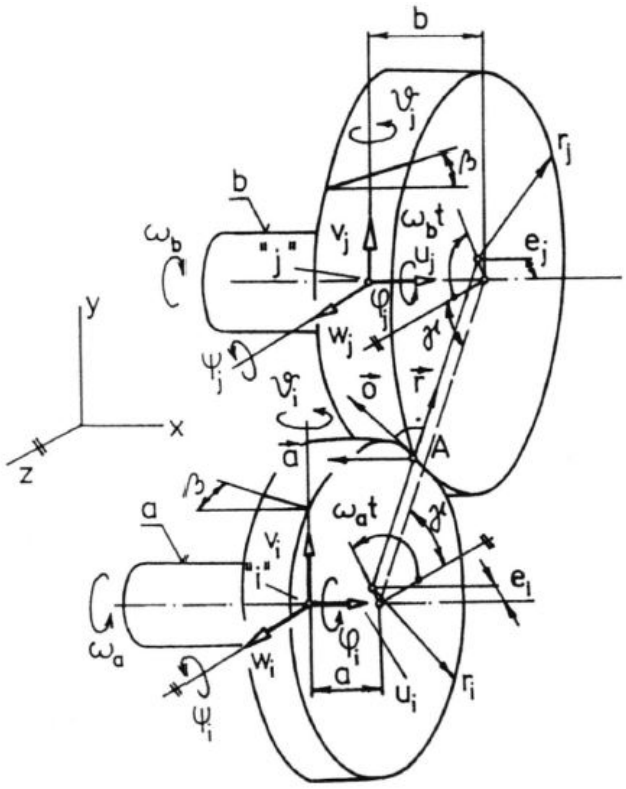

Fig. 6: Scheme of gearing coupling [6]

Non-linearities and other gearing phenomena

In the mathematical model of gearing we can consider the following phenomena:

- *Kinematic transmission error*
  It represents the manufacturing inaccuracy of the gears, which is at nominal static load considered to be periodic function of time with the period of meshing gears. In the computational model, we will simulate kinematic transmission error by inserting a fictitious wedge of width $\Delta_z(t)$ between the ideally meshing gears [6]. This periodic function can be approximated by Fourier series [6]

$$\Delta_z(t) = \sum_{k=1}^{K} \left(\Delta_{z,k}^C \cos k\omega_z t + \Delta_{z,k}^S \sin k\omega_z t \right), \tag{2.4.6}$$

  where ω_z is a meshing frequency, $\Delta_{z,k}^S$ is sinus part and $\Delta_{z,k}^C$ is cosinus part of the kinematic transmission error.

- *Time-varying meshing stiffness*
  This phenomenon is a source of the parametric excitation due to the change of number of tooth pairs in mesh. The modelling of gear stiffness has been developing many years as well as the mathematical model itself. In the first publications, the meshing stiffness was considered to be constant, but new more accurate models are being created nowadays. The most common approaches to model time-varying

meshing stiffness are analytical and numerical approaches.

a) The analytical approach
The stiffness of a particular tooth pair is considered to be periodic and it is generally influenced by the tooth profile, profile error, gear contact ratio and lubricant properties in gearing. This periodic function can be approximated by Fourier series [6]

$$k_z(t) = k_{z,0} + \sum_{n=1}^{N} \left(k_{z,n}^C \cos n\omega_z t + k_{z,n}^S \sin n\omega_z t \right), \tag{2.4.7}$$

where ω_z is a meshing frequency, $k_{z,n}^S$ is a sinus part and $k_{z,n}^C$ is cosinus coefficient of Fourier series. Zero coefficient of Fourier series $k_{z,0}$ can be expressed as

$$k_{z,0} = k_z^p + \Delta k_z(\epsilon_\gamma - p), \tag{2.4.8}$$

where k_z^p is a stiffness of p-th tooth in contact and ϵ_γ is a gear contact ratio.

b) The numerical approach
Owing to the complex geometries and the use of empirical values, analytical model is not precise to perform the exact calculation, that is the time when numerical approach is being used. This approach is based on the finite element method (FEM). In [7], there is this approach presented very precisely with the comparison of analytical approach.

- *Gear backslash non-linearity*

According to the external static load we can distinguish three different phases of gear mesh. Most of publications which deal with the gear dynamics assume ideal meshing gears with no interruption (a). With a relatively small external static load, the contact may be interrupted, and the relative motion (gear deformation d_z) can interfere within the backlash (b) or there may be a delimitation of the backslash u_z which cause the inverse gear mesh (c). These phases cause a change in overall gearing force (fig. 7), which depends on gear deformation. The non-linear part of

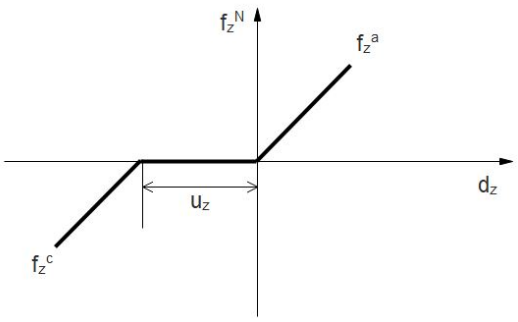

Fig. 7: Gearing non-linear force

the force can be expressed as [6]

$$f_z^N(d_z,t) = -k_z(t)d_z\mathrm{H}(-d_z) + k_z(t)(d_z+u_z)\mathrm{H}(-d_z-u_z), \tag{2.4.9}$$

where u_z is the gear backslash and H is the Heaviside function.

Total gearing force of this phenomena
The total gearing force which is applied on the s-subsystem can be expressed as [6]

$$\mathbf{f}_s^G = \pm\sum_z \hat{\boldsymbol{\delta}}_z F_z(t,d_z,\dot{d}_z), \tag{2.4.10}$$

where minus is corresponding to pinion and plus to wheel, $\hat{\boldsymbol{\delta}}$ is an extended vector of the geometric parameters of pinion or wheel, which is placed in the i-node of the subsystem $\hat{\boldsymbol{\delta}}_z = [...\boldsymbol{\delta}_i^T...]^T$. The total gearing force of the whole system of n degree of freedom with Z gearings can be expressed as

$$\mathbf{f}^G = \underbrace{\sum_{z=1}^{Z}\left(k_z(t)\Delta_z(t) + b_z\dot{\Delta}_z(t)\right)\mathbf{c}_z}_{\mathbf{f}_G^I} + \underbrace{\sum_{z=1}^{Z} f_z^N(d_z,t)\mathbf{c}_z}_{\mathbf{f}_G^N}, \tag{2.4.11}$$

where the vector of all geometric parameters can be for gears placed in i- and j- node written in this form [6]

$$\mathbf{c}_z = [... - \boldsymbol{\delta}_i^T ... \boldsymbol{\delta}_j^T ...]^T. \tag{2.4.12}$$

2.5 Mathematical model of single stage gearbox

Let us suppose a single stage isolated gearbox with two shafts (fig. 8).

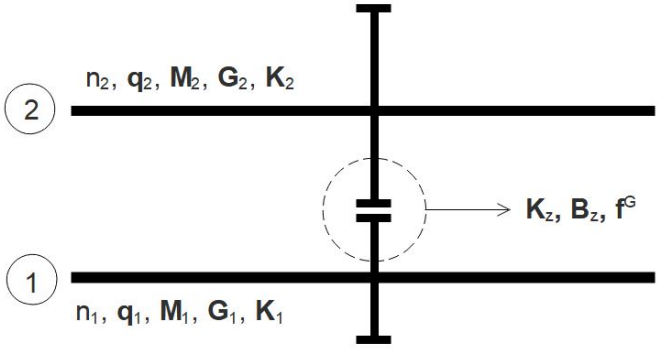

Fig. 8: Single speed gearbox

This system can be divided into 2 subsystems, which are represented by 2 shafts. Both subsystems are characterized by the degree of freedom n_s, vector of general coordinates $\mathbf{q}_s$, mass matrix $\mathbf{M}_s$, gyroscopic matrix $\mathbf{G}_s$ ans stiffness matrix $\mathbf{K}_s$. Mathematical model

of the subsystem s can be expressed as (2.1.11). These subsystems are connected via gearing which is characterized by the stiffness matrix $\mathbf{K}_z$, damping matrix $\mathbf{B}_z$ and vector of gearing forces $\mathbf{f}^G$. If we create a vector of general coordinates $\mathbf{q}(t) = [\mathbf{q}_1, \mathbf{q}_2]^T$ and degree of freedom $n = n_1 + n_2$, we can then express the mathematical model of whole gearbox as

$$\begin{bmatrix} \mathbf{M}_1 & \mathbf{0} \\ \mathbf{0} & \mathbf{M}_2 \end{bmatrix} \begin{bmatrix} \ddot{\mathbf{q}}_1 \\ \ddot{\mathbf{q}}_2 \end{bmatrix} + \left\{ \omega_0 \begin{bmatrix} \mathbf{G}_1 & \mathbf{0} \\ \mathbf{0} & \mathbf{G}_2 \end{bmatrix} + \mathbf{B}_z \right\} \begin{bmatrix} \dot{\mathbf{q}}_1 \\ \dot{\mathbf{q}}_2 \end{bmatrix} + \left\{ \begin{bmatrix} \mathbf{K}_1 & \mathbf{0} \\ \mathbf{0} & \mathbf{K}_2 \end{bmatrix} + \mathbf{K}_z \right\} \begin{bmatrix} \mathbf{q}_1 \\ \mathbf{q}_2 \end{bmatrix} = \mathbf{f}^G \quad (2.5.1)$$

If we want to include the effect of journal bearings, we just add a vector of hydrodynamic forces

$$\mathbf{f}^H = \begin{bmatrix} \mathbf{f}_{H,1} \\ \mathbf{f}_{H,2} \end{bmatrix}, \quad (2.5.2)$$

to the right side of the mathematical model (2.5.1), where vector of hydrodynamic forces $\mathbf{f}_{H,s}$ for subsystem s is in form (2.3.9). This derivation can be generalized to multiple shafts.

3 Dynamic analysis of rotating systems

3.1 State space model

Let us consider a mathematical model of rotating system in general form [6]

$$\mathbf{M}\ddot{\mathbf{q}}(t) + \mathbf{B}\dot{\mathbf{q}}(t) + \mathbf{K}\mathbf{q}(t) = \mathbf{f}(t), \tag{3.1.1}$$

which is the system of n second order differential equations with initial conditions

$$\mathbf{q}(0) = \mathbf{q}_0, \qquad \dot{\mathbf{q}}(0) = \dot{\mathbf{q}}_0, \tag{3.1.2}$$

When we solve this system of equations, we get a vector of generalized displacements $\mathbf{q}(t)$ and vector of generalized velocities $\dot{\mathbf{q}}(t)$ for a time within interval $t = [0, T]$. We have to transform this system of n second order equations to the system of $2n$ first order equations. To do so, we need to attach to the model (3.1.1) an identity expressed as [6]

$$\begin{aligned} \mathbf{M}\ddot{\mathbf{q}} + \mathbf{B}\dot{\mathbf{q}} + \mathbf{K}\mathbf{q} &= \mathbf{f} \\ \mathbf{M}\dot{\mathbf{q}} - \mathbf{M}\dot{\mathbf{q}} &= \mathbf{0}. \end{aligned} \tag{3.1.3}$$

Matrix form of this system is

$$\underbrace{\begin{bmatrix} \mathbf{M} & \mathbf{0} \\ \mathbf{0} & \mathbf{M} \end{bmatrix}}_{\mathbf{N}} \underbrace{\begin{bmatrix} \ddot{\mathbf{q}} \\ \dot{\mathbf{q}} \end{bmatrix}}_{\dot{\mathbf{u}}} + \underbrace{\begin{bmatrix} \mathbf{B} & \mathbf{K} \\ -\mathbf{M} & \mathbf{0} \end{bmatrix}}_{\mathbf{P}} \underbrace{\begin{bmatrix} \dot{\mathbf{q}} \\ \mathbf{q} \end{bmatrix}}_{\mathbf{u}} = \underbrace{\begin{bmatrix} \mathbf{f} \\ \mathbf{0} \end{bmatrix}}_{\tilde{\mathbf{f}}}, \tag{3.1.4}$$

where $\mathbf{u}(t)$ is the state space, the system can be written as

$$\mathbf{N}\dot{\mathbf{u}} + \mathbf{P}\mathbf{u} = \tilde{\mathbf{f}}. \tag{3.1.5}$$

If we multiply the system (3.1.5) with $\mathbf{N}^{-1}$ from the left

$$\dot{\mathbf{u}} = \underbrace{-\mathbf{N}^{-1}\mathbf{P}}_{\mathbf{A}}\mathbf{u} + \underbrace{\mathbf{N}^{-1}\tilde{\mathbf{f}}}_{\mathbf{F}}, \tag{3.1.6}$$

the system is in this form [6]

$$\dot{\mathbf{u}} = \mathbf{A}\mathbf{u} + \mathbf{F}, \tag{3.1.7}$$

where the system matrix $\mathbf{A}$ and the vector of external forces $\mathbf{F}$ can be expressed as [6]

$$\mathbf{A} = \begin{bmatrix} -\mathbf{M}^{-1}\mathbf{B} & -\mathbf{M}^{-1}\mathbf{K} \\ \mathbf{I} & \mathbf{0} \end{bmatrix}, \qquad \mathbf{F} = \begin{bmatrix} \mathbf{M}^{-1}\mathbf{f} \\ \mathbf{0} \end{bmatrix}. \tag{3.1.8}$$

With the initial conditions

$$\mathbf{u}(0) = \begin{bmatrix} \dot{\mathbf{q}}_0 \\ \mathbf{q}_0 \end{bmatrix}, \tag{3.1.9}$$

we can then solve the system (3.1.7) by using Runge-Kutta method, which is the part of MATLAB library as a function called *ode*45.

3.2 Modal analysis

Modal analysis method has been developing for years. This theory is taken from [6] and [2]. For this purpose, we have to use the mathematical model (3.1.1) without forces, i.e. $\mathbf{f}(t) = \mathbf{0}$. Let us consider, that the model consist of asymmetrical matrices. In this case, we use the $2n$ model (3.1.5) and its adjoint formulation

$$\mathbf{N}\dot{\mathbf{u}}(t) + \mathbf{P}\mathbf{u}(t) = \mathbf{0}, \qquad \mathbf{N}^T\dot{\mathbf{w}}(t) + \mathbf{P}^T\mathbf{w}(t) = \mathbf{0}, \tag{3.2.1}$$

where $\mathbf{u}(t)$ and $\mathbf{w}(t)$ are the vectors of state space and adjuncted state space. Suppose the solution of these system of equations in this form

$$\mathbf{u}(t) = \mathbf{u}\mathrm{e}^{\lambda t}, \qquad \mathbf{w}(t) = \mathbf{w}\mathrm{e}^{\lambda t}, \tag{3.2.2}$$

where λ is a number and $\mathbf{u}$,$\mathbf{w}$ are vectors. If we put these vectors (3.2.2) in equations (3.2.1) we then get

$$(\lambda\mathbf{N} + \mathbf{P})\mathbf{u} = \mathbf{0}, \qquad (\lambda\mathbf{N}^T + \mathbf{P}^T)\mathbf{w} = \mathbf{0}. \tag{3.2.3}$$

For non-trivial roots of both equations (3.2.3) must be applied

$$\det(\lambda\mathbf{N} + \mathbf{P}) = 0, \qquad \det(\lambda\mathbf{N}^T + \mathbf{P}^T) = 0. \tag{3.2.4}$$

From these systems of equations, we can get eigenvalues in general form

$$\lambda_\nu = \alpha_\nu + \mathrm{i}\beta_\nu, \qquad \nu = 1, 2, \ldots, 2n \tag{3.2.5}$$

If we then put these eigenvalues to the (3.2.3) we get the eigenvectors $\mathbf{u}$ and $\mathbf{w}$. Eigenvectors must be normed [6]. The norm can be expressed as [6]

$$\mathbf{W}^T\mathbf{N}\mathbf{U} = \mathbf{I}, \qquad \mathbf{W}^T\mathbf{P}\mathbf{U} = -\mathbf{\Lambda}, \tag{3.2.6}$$

where $\mathbf{W}$ and $\mathbf{U}$ are the modal matrices, which consist of the transponed eigenvectors and $\mathbf{\Lambda} = \mathrm{diag}(\lambda_\nu)$ is the diagonal matrix of eigenvalues.

Campbell diagram

Campbell diagram is being used in rotordynamics to find critical frequencies. For these type of systems, the natural frequencies often depend on the rotation rates ω_0 due to the induced gyroscopic effects or variable hydrodynamic conditions in fluid bearings. The gyroscopic effects are included in the gyroscopic matrix $\mathbf{G}$ of the mathematical model

$$\mathbf{M}\ddot{\mathbf{q}} + (\mathbf{B} + \omega_0\mathbf{G})\,\dot{\mathbf{q}} + \mathbf{K}\mathbf{q} = \mathbf{f}. \tag{3.2.7}$$

The concept of critical frequencies may be conceived generally as any condition in which the nominal angular velocity equals one of its natural frequencies [4]. The Campbell diagram can be created analytically or experimentally [4]. The analytical method is based on modal analysis. For each nominal angular velocity, natural frequencies are calculated and displayed depending on the nominal velocity. The example of the Campbell diagram is in fig. 9, where you can see how natural frequencies depend on the nominal angular velocity.

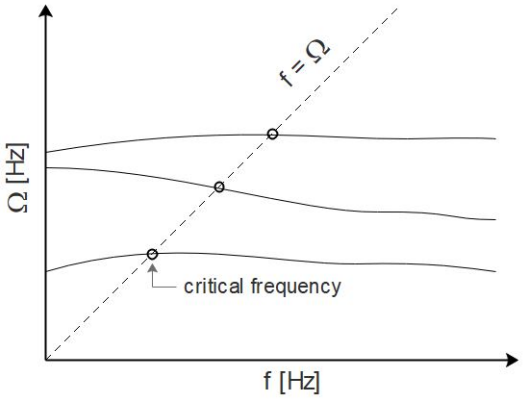

Fig. 9: Campbell diagram

Stability analysis

Stability of rotating systems depends on the real parts of the eigenvalues (3.2.5). There could be three possibilities [2]:

- Asymptotic stable
  Real parts of all eigenvalues are in the left side of the complex sub-area ($\alpha_\nu < 0$).
- Non-stable type flutter
  At least one pair of complex conjugate eigenvalues lies in the positive complex sub-area.
- Non-stable type divergency
  At least one real eigenvalue is positive ($\alpha_\nu > 0$)

The stability analysis can be also done by using *modal damping ratio* which can be expressed as [2]

$$D_\nu = -\frac{\alpha_\nu}{|\lambda_\nu|}. \tag{3.2.8}$$

The system is then non-stable when the value of (3.2.8) is negative.

Stability analysis of fluid bearings is a crucial part of determining its non-linearities. In a fluid bearing, non-stability called *oil whirl* can develop. Oil whirl can lead to another non-stability called *oil whip*. These non-linearities might be caused by [14], [4]:

- High angular velocity of the rotor.
- Large bearing clearance.
- Oil pressure fluctuation .
- Change of physical properties of oil film.
- Significant gyroscopic forces.

The instability oil whirl causes self-excited vibrations of the rotor at roughly 0.42–0.49 of the shaft speed [14]. Oil whip arises when the whirl frequency is close to some of the system natural frequency [14]. It is useful to visualize these phenomena using frequency analysis - Fourier transformation of bearing displacement for several shaft rotation values. The result of this approach is called *waterfall diagram* (fig. 10)

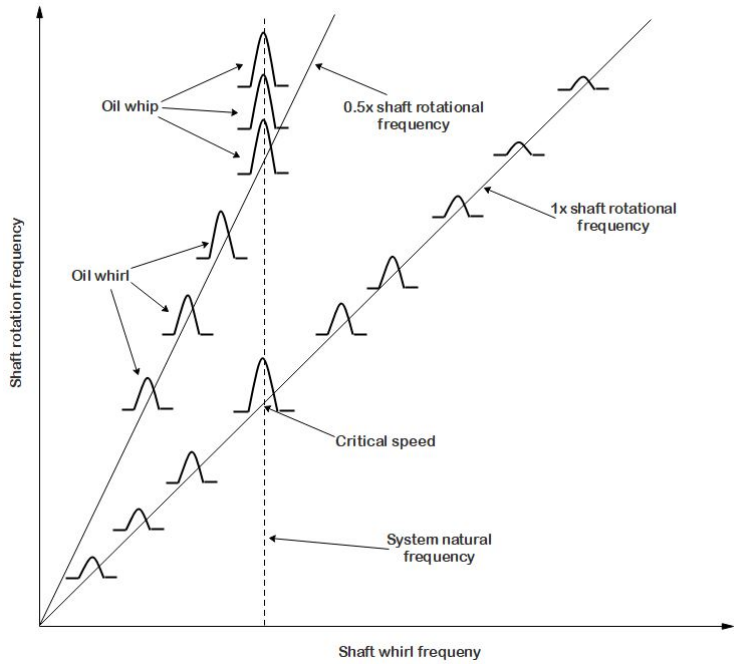

Fig. 10: Waterfall diagram

In practical applications, the waterfall diagram is created using fast Fourier transform algorithm (fft) of a time depending signal, which can be observed numerically or experimentally. Fast Fourier transform algorithm is a part of a MATLAB function library.

3.3 Modal synthesis

Mathematical models of dynamic systems with a lot of degrees of freedom are represented by many differential equations. It takes a lot of time to solve these system of equations. For that reason, modal reduction takes place. One of the modal reduction method is a modal synthesis that has been developing on the department of mechanics in Pilsen. Modal synthesis theory written in this paper is taken from [6]. Imagine j-subsystem of a shaft with a disc supported by journal bearings like in picture fig. 8, that is part of connected system of N shafts. Each subsystem has n_j degrees of freedom and the whole system has n degrees of freedom. Mathematical model of this subsystem can be written in this form

$$\mathbf{M}_j\ddot{\mathbf{q}}_j(t) + \omega_j\mathbf{G}_j\dot{\mathbf{q}}_j(t) + \mathbf{K}_j\mathbf{q}_j(t) = \mathbf{f}_H^{(j)} + \mathbf{f}_G^{(j)} + \mathbf{f}_C^{(j)}, \tag{3.3.1}$$

where all variables are described in chapter 2 except for vector of coupled forces $\mathbf{f}_C^{(j)}$, which represents the coupling with other subsystems. If we create a global vector of generalized coordinates

$$\mathbf{q}(t) = [\dots, \mathbf{q}_j^T(t), \dots]^T \in \mathbb{R}^n, \tag{3.3.2}$$

we can then write vectors on the right side of the global mathematical model in form

$$\mathbf{f}_H = \begin{bmatrix} \vdots \\ \mathbf{f}_H^{(j)} \\ \vdots \end{bmatrix}, \quad \mathbf{f}_G = \begin{bmatrix} \vdots \\ \mathbf{f}_G^{(j)} \\ \vdots \end{bmatrix}, \quad \mathbf{f}_C = \begin{bmatrix} \vdots \\ \mathbf{f}_C^{(j)} \\ \vdots \end{bmatrix}. \tag{3.3.3}$$

Accoring to (2.4.11), we can express the global coupling force as [6]

$$\mathbf{f}_C = -\mathbf{K}_C\mathbf{q}(t) - \mathbf{B}_C\dot{\mathbf{q}}(t) + \mathbf{f}_C^N(\mathbf{q}, \dot{\mathbf{q}}, t) + \mathbf{f}_I(t). \tag{3.3.4}$$

Modal synthesis method consists of following tasks. First of all, modal analysis of each j-subsystem needs to be done. Modal analysis is performed for undamped, non-rotating model

$$\mathbf{M}_j\ddot{\mathbf{q}}_j(t) + \mathbf{K}_j\mathbf{q}_j(t) = \mathbf{0}. \tag{3.3.5}$$

Similarly to chapter 3.2, we can then perform a modal analysis. But in case of undamped and non-rotating system, modal analysis is based on this equation [6]

$$(\mathbf{K}_j - \Omega_{i,j}^2\mathbf{M}_j)\mathbf{v}_{i,j} = \mathbf{0}, \tag{3.3.6}$$

where $\Omega_{i,j}$ is i-eigenvalue and $\mathbf{v}_{i,j}$ is i-eigenvector of j-subsystem. We can than also create modal matrices, which in this case can be expressed as

$$\mathbf{V}_j = \begin{bmatrix} \vdots & \vdots & \vdots \\ \dots & \mathbf{v}_{i,j} & \dots \\ \vdots & \vdots & \vdots \end{bmatrix} \in \mathbb{R}^{n_j,n_j}, \quad \mathbf{\Lambda}_j = \begin{bmatrix} \Omega_{1,j} & & \\ & \ddots & \\ & & \Omega_{n_j,j} \end{bmatrix} \in \mathbb{R}^{n_j,n_j}. \tag{3.3.7}$$

Again, these modal matrices need to be normed. In this case, the norm can be expressed as [6]

$$\mathbf{V}_j^T \mathbf{M}_j \mathbf{V}_j = \mathbf{I}_j, \quad \mathbf{V}_j^T \mathbf{K}_j \mathbf{V}_j = \mathbf{\Lambda}_j, \tag{3.3.8}$$

The second step of the modal synthesis is to split modal matrices to m_j-master and s_j-slave components [6]

$$\mathbf{V}_j = \begin{bmatrix} {}^{m_j}\mathbf{V}_j & \dots & {}^{s_j}\mathbf{V}_j \end{bmatrix}, \quad \mathbf{\Lambda}_j = \begin{bmatrix} {}^{m_j}\mathbf{\Lambda}_j & & \\ & \ddots & \\ & & {}^{s_j}\mathbf{\Lambda}_j \end{bmatrix}, \tag{3.3.9}$$

where master parts of the modal matrices are

$${}^{m_j}\mathbf{V}_j \in \mathbb{R}^{n_j,m_j}, \quad {}^{m_j}\mathbf{\Lambda}_j \in \mathbb{R}^{m_j,m_j}, \tag{3.3.10}$$

The third step of proposed method is to perform modal transformation [6]

$$\mathbf{q}_j(t) = {}^{m_j}\mathbf{V}_j \mathbf{x}_j(t), \tag{3.3.11}$$

where $\mathbf{x}_j(t)$ is the vector of modal coordinates. If we put the (3.3.11) to (3.3.1) we get

$$\mathbf{M}_j \, {}^{m_j}\mathbf{V}_j \ddot{\mathbf{x}}_j(t) + \omega_j \mathbf{G}_j \, {}^{m_j}\mathbf{V}_j \dot{\mathbf{x}}_j(t) + \mathbf{K}_j \, {}^{m_j}\mathbf{V}_j \mathbf{x}_j(t) = \mathbf{f}_H^{(j)} + \mathbf{f}_G^{(j)} + \mathbf{f}_C^{(j)}. \tag{3.3.12}$$

If we multiply the equation (3.3.12) by transposed master modal matrix (3.3.10) from left and if we use norm (3.3.8) we than get reduced mathematical model of m_j differential equations of j- subsystem

$$\ddot{\mathbf{x}}_j(t) + \omega_j \, {}^{m_j}\mathbf{V}_j^T \mathbf{G}_j \, {}^{m_j}\mathbf{V}_j \dot{\mathbf{x}}_j(t) + \, {}^{m_j}\mathbf{\Lambda}_j \mathbf{x}_j(t) = \, {}^{m_j}\mathbf{V}_j^T (\mathbf{f}_H^{(j)} + \mathbf{f}_G^{(j)} + \mathbf{f}_C^{(j)}). \tag{3.3.13}$$

If we than create a global vector of modal coordinates in form

$$\mathbf{x}(t) = \begin{bmatrix} \vdots \\ x_j(t) \\ \vdots \end{bmatrix} \in \mathbb{R}^m, \quad m = \sum_{j=1}^{N} m_j, \tag{3.3.14}$$

global modal matrices and global gyroscopic matrix [6]

$$\mathbf{V} = \begin{bmatrix} {}^{m_1}\mathbf{V}_1 & & \\ & \ddots & \\ & & {}^{m_N}\mathbf{V}_N \end{bmatrix} \in \mathbb{R}^{n,m}, \quad \mathbf{\Lambda} = \begin{bmatrix} {}^{m_1}\mathbf{\Lambda}_1 & & \\ & \ddots & \\ & & {}^{m_N}\mathbf{\Lambda}_N \end{bmatrix} \in \mathbb{R}^{m,m}, \tag{3.3.15}$$

$$\mathbf{G} = \begin{bmatrix} \frac{\omega_1}{\omega_0}\ {}^{m_1}\mathbf{V}_1^T\mathbf{G}_1\ {}^{m_1}\mathbf{V}_1 & & \\ & \ddots & \\ & & \frac{\omega_N}{\omega_0}\ {}^{m_N}\mathbf{V}_N^T\mathbf{G}_N\ {}^{m_N}\mathbf{V}_N \end{bmatrix} \in \mathbb{R}^{m,m}, \tag{3.3.16}$$

we can then, according to the global coupling forces (3.3.4), express the global reduced mathematical model of the whole system as [6], [2]

$$\ddot{\mathbf{x}}(t) + (\omega_0\mathbf{G} + \mathbf{V}^T\mathbf{B}_C\mathbf{V})\dot{\mathbf{x}}(t) + (\mathbf{\Lambda} + \mathbf{V}^T\mathbf{K}_C\mathbf{V})\mathbf{x}(t) = \mathbf{V}^T[\mathbf{f}_C^N(\mathbf{q}, \dot{\mathbf{q}}, t) + \mathbf{f}_I(t) + \mathbf{f}_H(\mathbf{q}, \dot{\mathbf{q}}, t)], \tag{3.3.17}$$

which represents system of m differential equations. Initial conditions are transformed exactly the same like the vector of global coordinates

$$\mathbf{q}(0) = \mathbf{V}\mathbf{x}(0), \tag{3.3.18}$$
$$\dot{\mathbf{q}}(0) = \mathbf{V}\dot{\mathbf{x}}(0). \tag{3.3.19}$$

3.4 Non-linear phenomena in dynamic systems

Dynamic analysis of non-linear systems differs from the linear systems in many things. Non-linear systems are characterized by [1], [6]

a) Sudden change of state when the system parameter is being constantly changed.

b) The source of unstable and unpredictability behaviour.

c) Chaotic behaviour.

These phenomena can be analysed using different tools, e.g. bifurcation diagram.

Bifurcation diagram

Bifurcation is one of the most characteristic phenomena of non-linear systems. A bifurcation is a sudden change of a state variable, i.e period doubling, which occurs when the control parameter is being changed. In the picture below, you can see that the period of the state variable doubled due to the change of the system parameter.

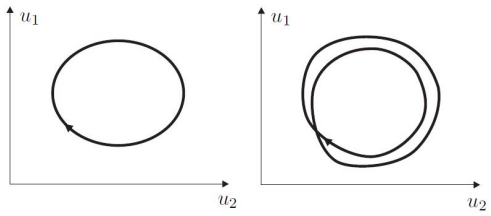

Fig. 11: Original period (left), doubled-period (right) [2]

A bifurcation diagram can be understood as a tool for visualisation of qualitative behaviour of the system. The behaviour can be usually characterized by a properly chosen system variable. There are different possibilities how to display the system response. In fig. 12, one can see a bifurcation diagram created for dynamic model of gearing with non-linear force.

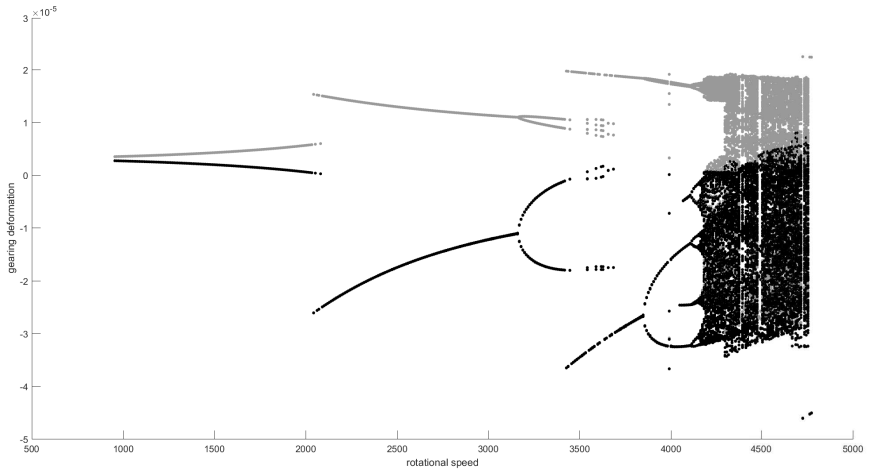

Fig. 12: Example of bifurcation diagram for a system with impacts

The fig. 12 shows the phenomena that can be observed in non-linear systems, where the gray color represents maximum and black color minimum of the tracked value. This diagram was created for non-linear system with impacts caused by the presence of the coupling clearance, where gearing systems considering the gear mesh clearance belong as well. The x-axis represents the angular velocity of the gears [rpm] and the y-axis represents gearing deformation [m]. You can see that at 3100 rpm the system doubled its period and this condition continued up to 4200 rpm where the system behaved chaotically.

4 Application

In this chapter, 3 applications of proposed methods will be presented. The 1st application is 2 DoF model of a rigid Laval rotor, the 2nd is a flexible rotor supported by fluid bearings and the last application is a single stage gearbox. With respect to the mathematical model of fluid film bearings presented in chapter 2.3, short bearings are used for all applications. With regard to this thesis, the 3rd application is the most important one. Both static and dynamic analyses will be performed using own created software in MATLAB.

4.1 Rigid Laval rotor

The very simple model of a Laval rotor supported by fluid film bearings is presented to show the basic dynamic behaviour of interaction between rotating shaft and fluid film bearings. The model of a rigid Laval rotor have been taken from [33]. A rigid Laval rotor is a rigid shaft with negligible weight and with a disc mounted in the middle of the shaft. The rotor is at both edges symmetrically supported by fluid bearings. With respect to symmetry, we can consider half the weight of the shaft to one of the bearing and simplified the model as a 2 DoF model shown in fig. 13. A rigid rotor of radius R and mass m is

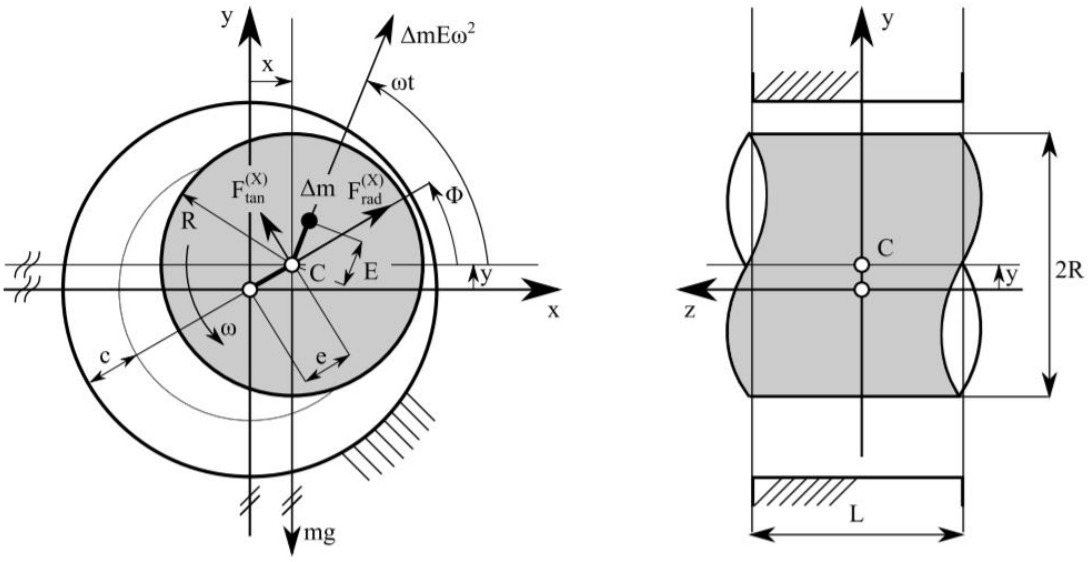

Fig. 13: Scheme of the model of Laval rotor supported by film fluid bearings [3]

rotating within the bearing housing with angular velocity ω. If the eccentricity e is zero, the clearance c represents the radial distance between the bearing and the rotor. Gravity force is applied to the rotor. Static unbalance ΔmE can be also considered. Horizontal displacement x and vertical displacement y of the shaft center C represent the generalized coordinates. Geometric properties are given by the length L, bearing diameter D and the clearance c. The oil presented in the bearing clearance has dynamic viscosity μ. The mathematical model of this system can be written in this form

$$\mathbf{M}\ddot{\mathbf{q}}(t) = \mathbf{f}_G + \mathbf{f}_e(t) + \mathbf{f}_{HD}(\mathbf{q}, \dot{\mathbf{q}}, t), \tag{4.1.1}$$

where $\mathbf{M} = \mathrm{diag}(m, m)$ is the mass matrix, $\mathbf{q}(t) = [x(t), y(t)]^T$ is the vector of general coordinates, $\mathbf{f}_G = [0, -mg]^T$ is the vector of the gravitational force, $\mathbf{f}_e(t) = \Delta m E[\cos \omega t, \sin \omega t]$ is the vector of the unbalance and $\mathbf{f}_{HD} = [F_{H,x}, F_{H,y}]^T$ is the vector of hydrodynamic forces (2.3.7). Parameters of this rotor-bearing model are listed in tab. 1. Both static and dynamic analysis will be performed numerically using MATLAB.

rotor mass	m	50 kg
rotor diameter	D	38 mm
bearing length	L	20 mm
clearance	c	50 μm
dynamic viscosity	η	10 $mPa \cdot s$

Tab. 1: Parameters of the model [33]

Static analysis

a) Determination of static equilibrium positions

For this analysis, we will consider the rotor to be perfectly balanced. The determination of static equilibrium positions, which solve the equation (2.3.11), is performed using MATLAB built-in function *fsolve* with an angular velocity in range $\omega \in (250; 12000)$ rpm. It is useful to display these positions using dimensionless approach with respect to clearance c. For parameters in tab. 1 you can see the static equilibrium positions depict in the fig. 14, where $\epsilon_x = x/c$ and $\epsilon_y = y/c$.

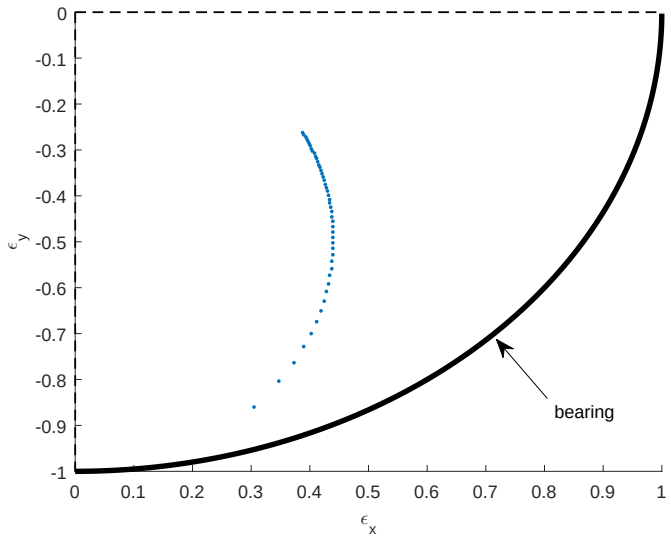

Fig. 14: Static equilibrium positions

You can see that as the speed increases, the rotor gradually floats up. But it is important to mention that we do not know anything about the stability of this system. At certain angular velocity, the system can become unstable as it is shown in the following chapters. The stability of equilibrium is lost by means of Hopf bifurcation, where the equilibrium loses its stability and a limit cycle is born [3].

b) Stiffness and damping coefficients

For the same range of angular velocity, we can determine stiffness and damping coefficients based on the approach in (2.3.14). These coefficients are displayed in fig. 15 and fig. 16.

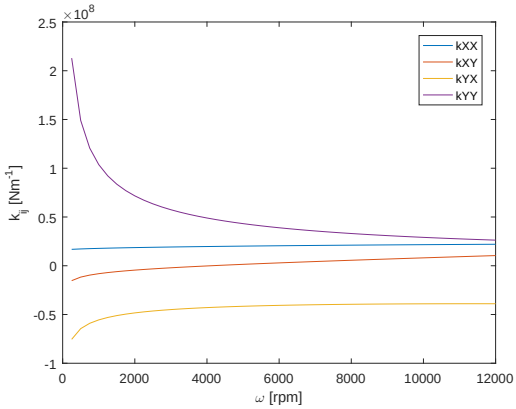

Fig. 15: Stiffness coefficients

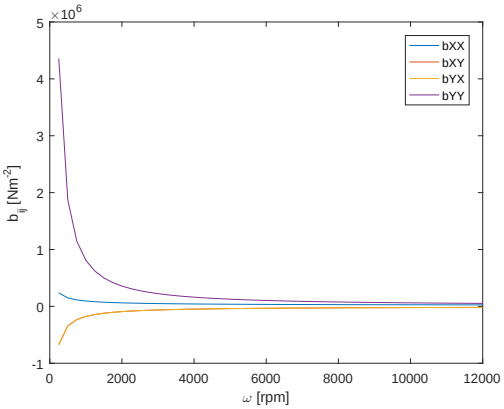

Fig. 16: Damping coefficients

It is obvious, that with increasing angular velocity, the absolute values of coefficients decrease due to hydrodynamics effect in fluid film. This phenomenon has a big influence on the general behaviour as well as on stability of the whole system.

c) Campbell diagram and stability analysis

With the knowledge of dynamic linearised coefficients, we can depict Campbell diagram and perform stability analysis using approach described in 3.2. For the Laval rotor and parameters in tab. 1, the Campbell diagram is displayed in fig. 17 and the stability analysis in fig. 18.

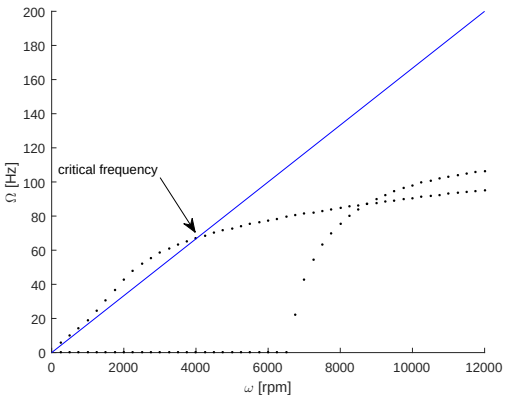

Fig. 17: Campbell diagram

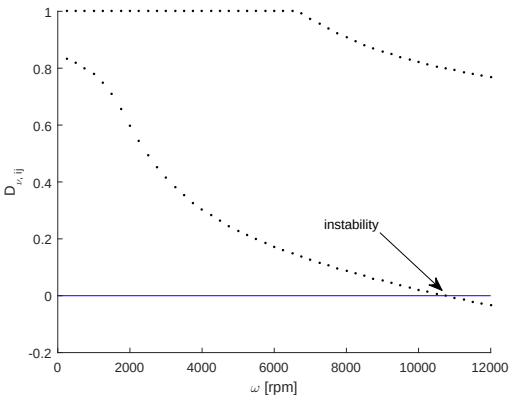

Fig. 18: Stability analysis

You can see, that in our case the system has 1 critical frequency at the angular velocity of the rotor $\omega_c = 4000$ rpm. Due to the dynamic change of the systems coefficients, the dynamic system lost its stability at around 10 800 rpm.

Dynamic analysis

d) Bifurcation diagram and frequency analysis

Using the approach described in 3.3 and 3.4 we can analyse non-linear phenomena in this system. These analyses were performed using MATLAB solver *ode45*. The system was excited by an unbalance force with the parameter $\Delta mE = 0.0012$. The value of the unbalance was determined in such a way to reveal oil film instabilites in the operating range of the rotor. In the fig. 19 you can see a bifurcation diagram of the ϵ_y variable based on changing the angular velocity ω [rpm]. The bifurcation diagram presented in fig. 19 displays maxima and minima of relative horizontal position of the rotor centre ϵ_y. The extremes of the mentioned quantity were captured from a steady-state behaviour of the rotor for at given rotor speed using numerical integration. In the fig. 20 there is the frequency analysis using waterfall diagram.

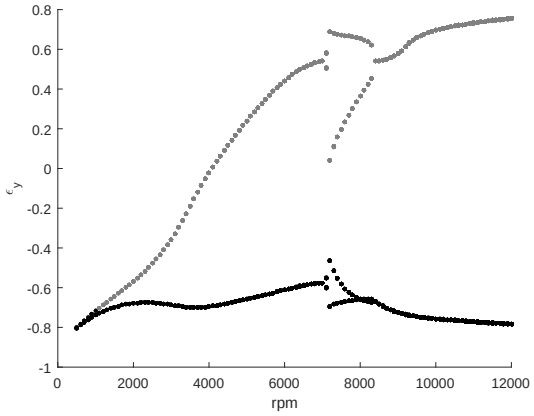

Fig. 19: Bifurcation diagram

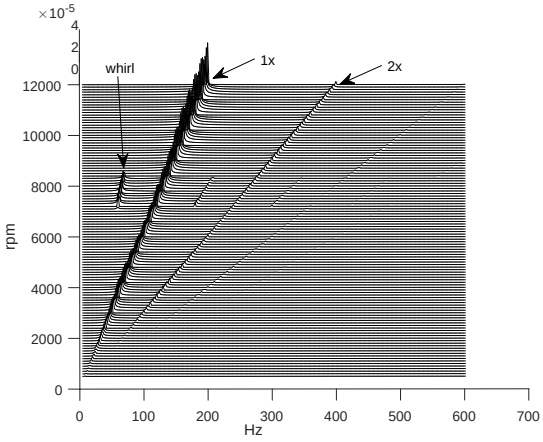

Fig. 20: Waterfall diagram

It is obvious that at about 7 250 rpm the period of the tracked variable ϵ_y doubled its period. As you can see from the fig. 20, this behaviour turned out to be *oil whirl*. As the angular velocity ω increased, the doubled period disappeared. In the fig. 21, you can see the orbit of the rotor at whirl frequency.

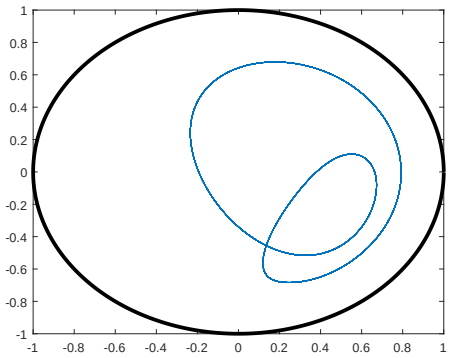

Fig. 21: Rotor steady state orbit corresponding to whirl motion

4.2 Rotor supported by fluid bearings

In previous section, there is described basic dynamic behaviour of the rigid rotor supported by fluid film bearings. In practical applications, the shaft has to be considered as flexible one. If the shaft is flexible, another type of instability can be exhibited - so called oil whip. To show the dynamic behaviour, a flexible rotor supported by two radial fluid film bearings is considered. The scheme of this system is depict in fig. 22.

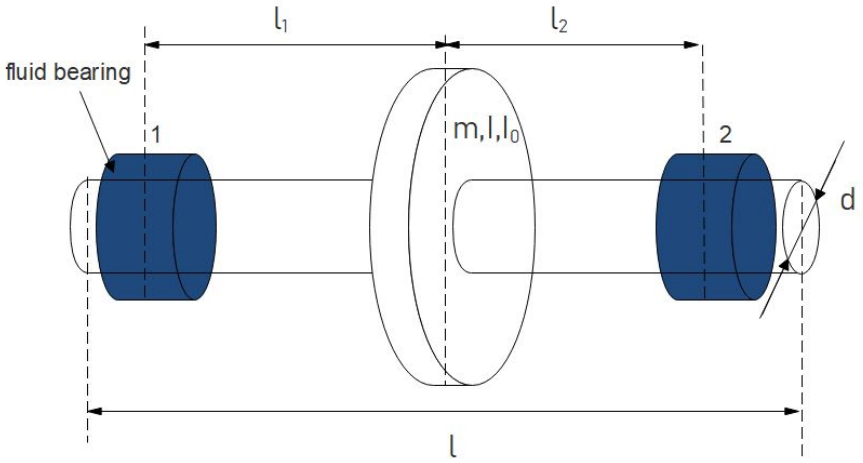

Fig. 22: Scheme of the rotor supported by journal bearings

Rotor is modelled using finite element method. The approach of modelling of each component is described in chapter 2. Parameters of the system are summarized in tab. 2.

Element	1	2	3-12	13	14
Diameter d_i [m]	0.03	0.03	0.04	0.03	0.03
Length l_i [m]	0.03	0.03	0.026	0.03	0.03

Tab. 2: Parameters of rotor elements

Shaft is made of steel with Young's modulus $E = 2.1 \cdot 10^{11}$ Pa, Poisson ratio $\nu = 0.3$, Shear modulus $G = 0.8 \cdot 10^{11}$ Pa and density $\rho = 7800$ kgm^3. The disc is characterized by mass $m = 2.65$ kg and moments of inertia $I = 0.0041$ kgm^2 $I_0 = 0.0079$ kgm^2. Both fluid bearings are characterized by length $L = 15$ mm, radial clearance $c = 0.9$ mm and dynamic viscosity $\mu = 0.07$ Pa $\cdot$ s. Lets consider that the disc is mounted in the middle of the shaft. Firstly, modal analysis and then both static and dynamic analyses will be performed on this system.

Modal analysis

Let us suppose isolated shaft with mounted disc in the middle of the rotor. Modal analysis of this non-rotating system is performed. First 16 frequencies of the modal analysis are listed in tab. 3.

Natural frequency	**Value [Hz]**	**Mode characteristics**
$f_1 - f_6$	0	Rigid system
$f_7 - f_8$	1182.4	Rotor bending
$f_9 - f_{10}$	2485.3	Rotor bending
f_{11-12}	5277.3	Rotor bending
f_{13}	5301.8	Dominant rotor torsion
f_{14}	5452.0	Dominant rotor torsion
f_{15-16}	5540.3	Rotor bending

Tab. 3: Modal analysis results

Static analysis

The static analysis consists of calculation of static equilibrium positions of rotating shaft in bearings, calculation of stiffness and damping coefficients and calculation of modal properties of the system. For this analysis, we will consider the rotor to be perfectly balanced.

a) Determination of static equilibrium positions
The determination of static equilibrium positions, which solve the system of equations (2.3.11), is performed using MATLAB built-in function *fsolve* within the range $\omega \in (1000, 15000)$ rpm. Dimensionless positions are displayed in fig. 23.

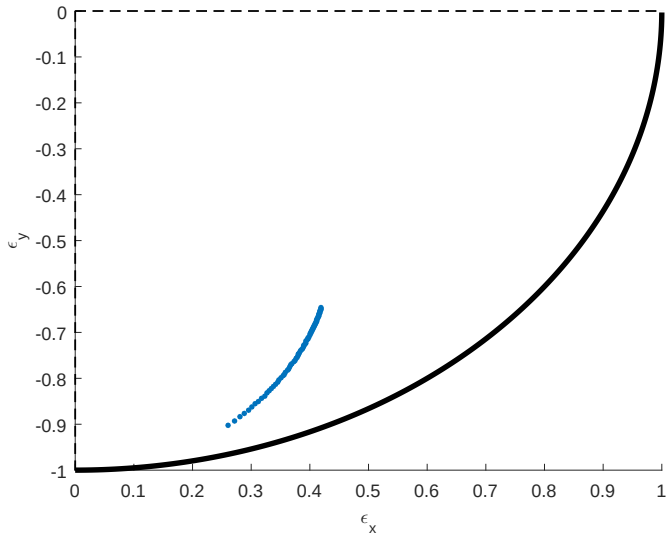

Fig. 23: Static equilibrium positions

Due to the position of the mounted disc, the static equilibrium positions are for both bearings identical.

b) Stiffness and damping coefficients

For the same range of angular velocity, we can determine stiffness and damping coefficients based on (2.3.14).

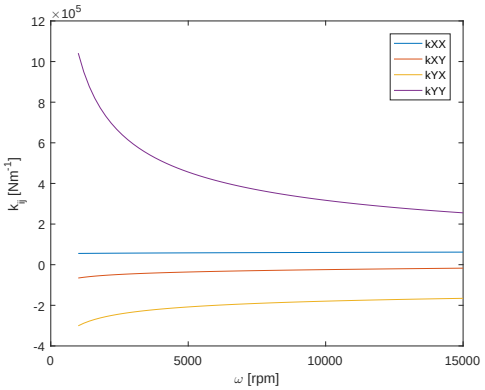

Fig. 24: Stiffness coefficients

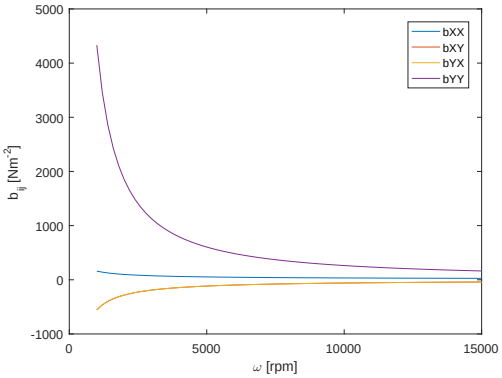

Fig. 25: Damping coefficients

As for the model of rigid Laval rotor, the dynamic coefficients of the bearings depend on the rotation speed of the shaft due to the hydrodynamic forces. In the fig. 24 and fig. 25 you can see that the values decrease with the increasing angular velocity of the rotor.

c) Campbell diagram and stability analysis
For the same range of angular velocity, we will examine the modal properties of the model. The Campbell diagram is created based on the modal properties of the rotor supported by fluid bearings, with the dynamic coefficients from fig. 24 and fig. 25. The Campbell diagram is for this case depict in fig. 26 and 27. The stability analysis is created using approach in chapter 3.2., where the value of modal damping ratio (3.2.8) is displayed.

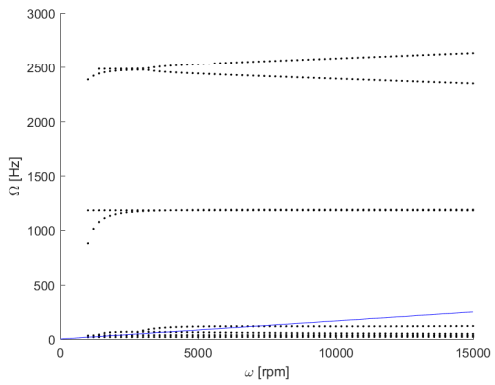

Fig. 26: Campbell diagram

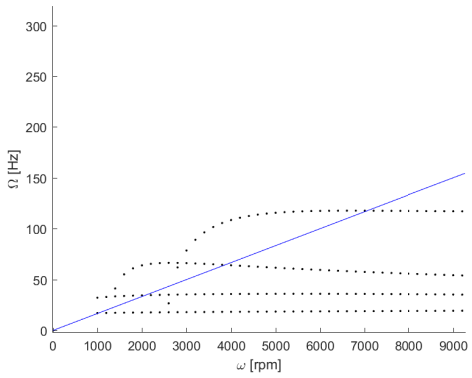

Fig. 27: Systems critical frequencies

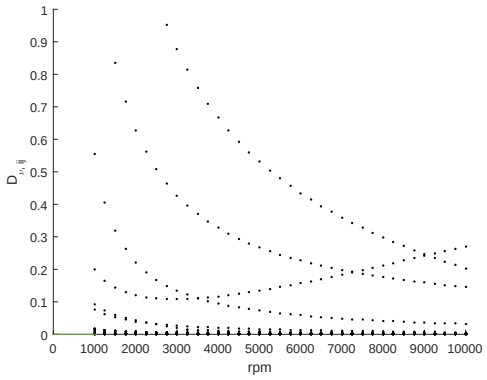

Fig. 28: Stability analysis of the rotor supported by fluid film bearings

According to the modal and stability analysis (fig. 28) we can definitely say, that the rotor has 4 very low critical speeds that can have huge impact on rotors dynamic behaviour. This condition may lead to vibration increasing while the rotor accelerates or decelerates. But the instability did not show according to stability analysis.

Dynamic analysis

To decrease computation time, we will use modal reduction method to decrease number of degrees of freedom of the model. The method combines both modal reduction and modal synthesis methods described in chapter 3.3. First, for each subsystem a transformation modal matrix is formed. This matrix is composed, in general, of first m eigen mode shapes of corresponding subsystem. In practical calculations, 25 eigen mode shapes were considered for each subsystem [1]. When using the reduced models, it is necessary to have a criterion which can help to decide on the reduced model accuracy. In the fig. 29 and fig. 30, there is a comparison of full and reduced model at different angular velocities of the rotor for dimensionless vertical displacement ϵ_y of the bearing.

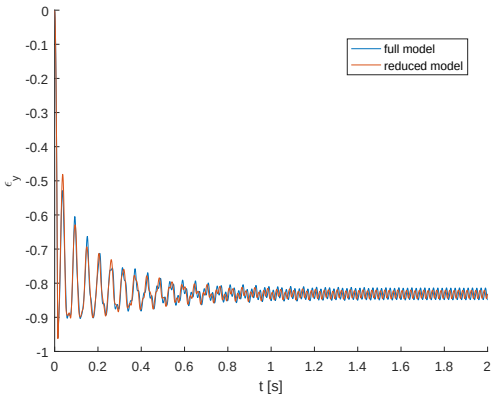

Fig. 29: Comparison of full and reduced model at ω =3000 rpm

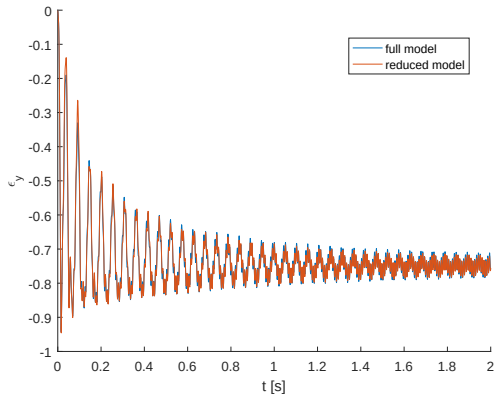

Fig. 30: Comparison of full and reduced model at ω =7000 rpm

According to the figures above, we can definitely say, that the reduced model very well describes the dynamic behaviour of the full model and we can use it for dynamic analysis

with reduction of computational time. The comparison of the computational time of the full and reduced model for proposed rotor speeds is listed in tab. 4.

	T [s] for $\omega = 3000$ rpm	T [s] for $\omega = 7000$ rpm
full model	995	1145
reduced model	39	43

Tab. 4: Comparison of computational time T of both full and reduced model for different rotor speeds

The dynamic analysis will be performed on a system with unbalance force applied on the disc (parameters are listed in the introduction of this chapter). During the dynamic simulation, we will observe vertical displacements of nodes located in one of the bearing (the model is symmetric) and disc positions. We will display bifurcation diagram and waterfall diagrams of these displacements at steady state using direct numerical integration. It means that the simulation time is chosen in such a way that the solution overcomes to steady-state motion. For the numerical integration, MATLAB function *ode*45 is used with absolute and relative tolerance set to 10^{-7}. The dynamic simulation will be performed for angular velocity of the rotor within range $\omega \in (1000, 10000)$ rpm. The results are displayed below.

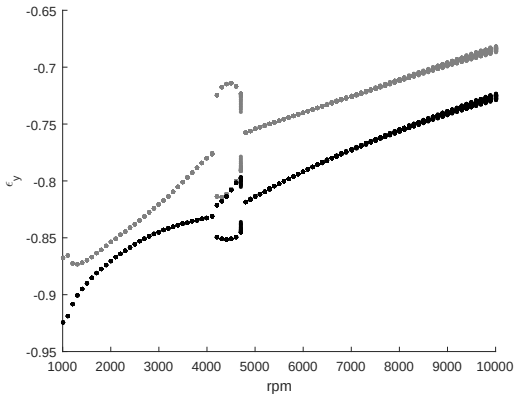

Fig. 31: Bifurcation diagram of dimensionless vertical displacement of the bearing

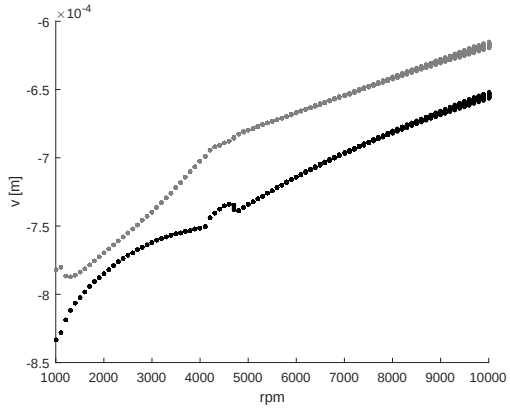

Fig. 32: Bifurcation diagram of vertical displacement of the disc

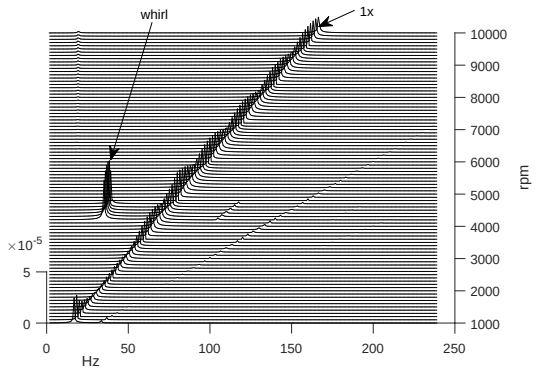

Fig. 33: Waterfall diagram of ϵ_y

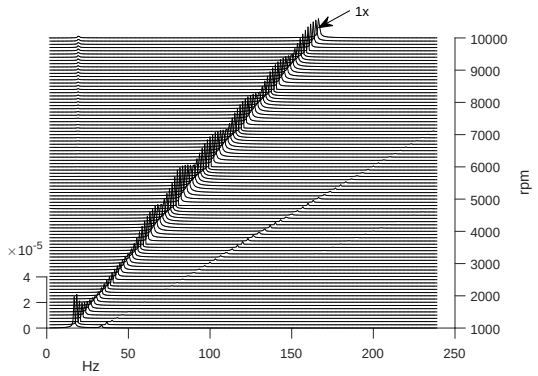

Fig. 34: Waterfall diagram of disc vertical displacement

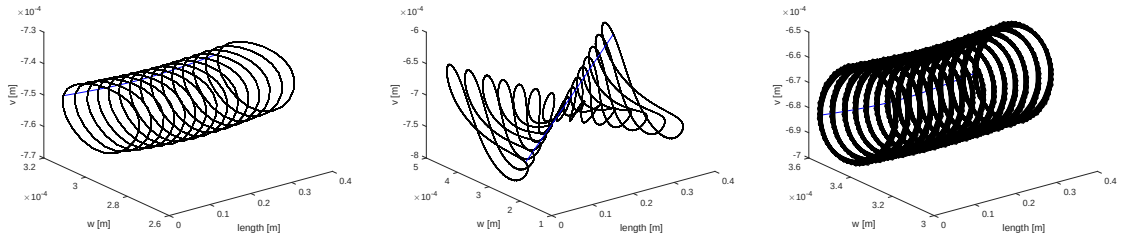

(a) (b) (c)

Fig. 35: Rotor orbits at specific velocity of the rotor (a) $\omega = 3000$ rpm, (b) $\omega = 4500$ rpm and (c) $\omega = 7000$ rpm

The response of the observed quantity forms a limit cycle, which is exhibited by the unbalance excitation. To capture the behaviour of the system, especially the displacement of the shaft in the bearing node, one can use the bifurcation diagram. The bifurcation diagram is formed by maxima and minima of the quantity (i.e. relative displacement of the bearings node in the vertical direction). From the fig. 33 you can see that the maxima and minima of the value ϵ_y are due to the unbalance force different. This is caused by a fact, that the rotor is circling around static equilibrium position (see fig. 35), the motion forms circular orbits. As the ω increased, the oil whirl occurred at ω= 4200 rpm. This type of instability caused self-excited vibrations of the rotor at 0.42–0.49 of the shaft speed (fig. 33) and doubling of the period of the tracked value. Orbits of the rotor at oil whirl frequency are displayed in fig. 35 (b). If the rotor operates at this frequency, this vibration may lead to bearing wear and possibly its destruction. Oil whirl frequency slightly showed in bifurcation diagram of the disc displacement because at that frequency the rotor vibrates mainly within bearing clearance. At 4900 rpm the oil whirl instability ends and the system becomes stable.

4.3 Gearbox

Finally, the dynamic analysis of a complex system will be performed. The mentioned models and methods for dynamic analysis will be applied to rotating part of a single stage gearbox. The system integrates fluid film bearing couplings and gear coupling. In general, both couplings have nonlinear characteristics. The scheme of the gearbox is depict in fig. 36. This gearbox was taken from [1], where dynamic analysis of this gearbox supported by ball bearings was performed. Let us consider that this gearbox is supported by fluid bearings.

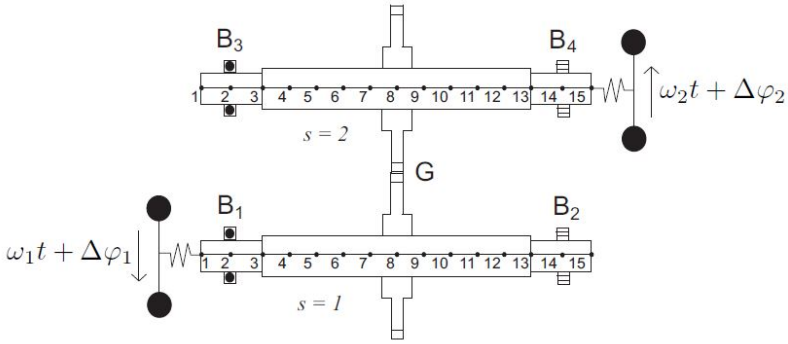

Fig. 36: Gearbox scheme [1]

It is a single stage gearbox, which consists of two flexible shafts connected via gearing G and supported by fluid bearings B_i $i = 1, 2, 3, 4$. The whole system can be divided into two main subsystems $s = 1, 2$. Parameters of both subsystems have been taken from chapter 4.2. Parameters of the gearing are listed in appendix.

Each shaft was modelled using finite element method. Both subsystems have fourteen shaft elements with fifteen nodes and 90 degrees of freedom. Each component of the subsystems was modelled using the approach described in chapter 2. Gears are considered to be perfectly rigid and fixed to shafts. Global mathematical model of this system can be written in form (2.5.1). Computational models were created in MATLAB .

For the next step, we should define boundary conditions for this system. Let us consider, that the driving and driven part of the drive system that is connected to the gearbox is replaced with rotating rigid discs. The driving and driven part is rotating with angular velocity ω_1 and ω_2 respectively. The loading torque that is transmitted trough the gearbox than causes a static torsional deformation $\Delta\varphi_1$ and $\Delta\varphi_2$ of the torsional couplings between shafts and the large rigid discs. The torque can be than expressed as $M_1 = \Delta\varphi_1 k_t$ and $M_2 = \Delta\varphi_2 k_t$ on driving and driven part respectively, where k_t is a torsional stiffness. The rest of the general coordinates φ_i^s in nodes than represent relative displacements with respect to rotation of the shafts. This approach can be used if we analyse the behaviour of the transmission at constant drive speed. If we want to analyse acceleration of the gearbox, we have to perform analysis without this torsional fixation.

We will perform modal, static and dynamic analyses of this system.

Modal analysis

First analysis that will be performed is modal analysis of both subsystems s and the whole gearbox. Results of this analysis will then be used for modal synthesis method, described in chapter 3. Results of modal analysis of the subsystem s are summarized in tab. 5.

Natural frequency	**Value [Hz]**	**Mode characteristics**
$f_1 - f_5$	0	Rigid system
f_6	104.1	Rigid system
$f_7 - f_8$	1182.4	Rotor bending
$f_9 - f_{10}$	2485.3	Rotor bending
f_{11-12}	5277.3	Rotor bending
f_{13}	5301.8	Dominant rotor torsion
f_{14}	5452.0	Dominant rotor torsion
f_{15-16}	5540.3	Rotor bending

Tab. 5: Modal analysis of isolated shaft s with rigid disc

The results from tab. 5 come from the subsystem with torsional fixation, so first five frequencies are zero. The sixth frequency represents torsional vibration of the torsional fixation. Doubled frequencies correspond to modes characterized by rotor bending. If it comes to modal analysis of the whole system, the results are summarized in tab. 6.

Natural frequency	**Value [Hz]**	**Mode characteristics**
$f_1 - f_4$	0	Rigid system
f_5	57.4	Tilting of the shafts to each other
f_6	104.1	Torsional deformation of the torsional fixation
f_7	1102.9	Bending of the whole system
$f_8 - f_{10}$	1182.4	Bending of each shaft separately, nodes in gearing
$f_{11} - f_{14}$	2485.3	Bending of each shaft separately
f_{15}	3479.9	Dominant gearing deformation
$f_{16} - f_{18}$	5277.3	Bending of each shaft separately, nodes in gearing

Tab. 6: Modal analysis of isolated shafts connected by gearing

Unlike the modal analysis of the model of isolated shaft (tab. 5) the model of shafts connected via gearing (tab. 6) has 4 zero frequencies which represent movement of the shafts as a rigid system even to each other. The 5th frequency is characterized by tilting of the shafts to each other due to the gearing coupling. The eigen mode shape corresponding to 6th eigen frequency is represented by torsional vibrating of the torsional fixation of both shafts. The eigen mode shape corresponding to 7th eigen frequency is specific by bending of the whole rotor-gearing system. The next couple of frequencies correspond mainly to the shape characterized by bending of the shafts relatively to each other.

Static analysis

Just like in the case of a rotor supported by fluid film bearings presented in chapter 4.2, we will perform static analysis, which focuses mainly on determining static equilibrium positions, stability analysis and Campbell diagram. Every proposed analysis depends on angular velocity of the shafts.

Based on previous analyses of rigid and flexible rotors supported by fluid film bearings, it has been shown that there exist some operational areas, where the system can exhibit equilibrium behaviour. If the system is operated under gravity load only, the response is formed by equilibrium up to the point, where it loses its stability and a limit cycle is formed. This loss of stability is induced by hydrodynamic forces in fluid film bearings. This behaviour may be observed in dynamic analysis.

All the analyses are performed numerically based on computational models created in MATLAB.

a) Determination of static equilibrium positions
Because of the fact, that the whole system is symmetric, equilibrium positions are for every bearing identical. Positions of shaft in bearing are displayed in fig. 37 using dimensionless values $\epsilon_y = y/c$ and $\epsilon_x = x/c$, where x, y are horizontal and vertical displacements of the rotor and c is the clearance.

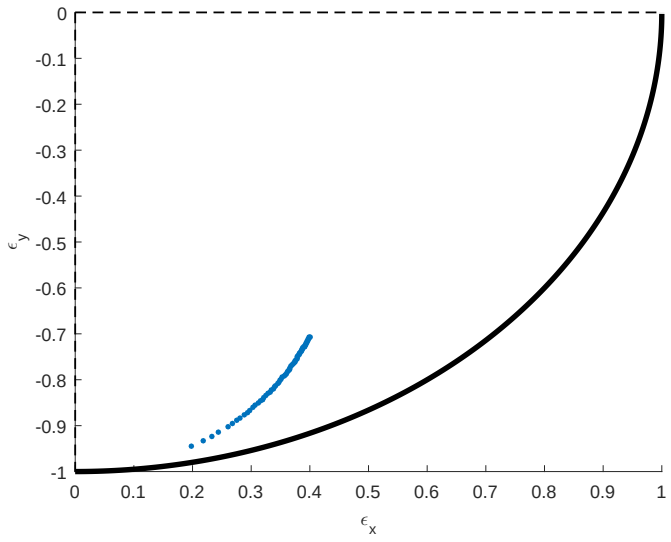

Fig. 37: Static equilibrium positions

b) Stiffness and damping coefficients
For the same range of angular velocity, we can determine stiffness and damping coefficients using (2.3.14), where the coefficients are determined using linear approximation of the hydrodynamic forces.

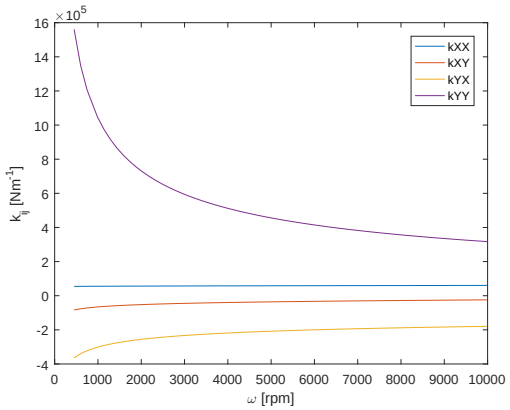

Fig. 38: Stiffness coefficients

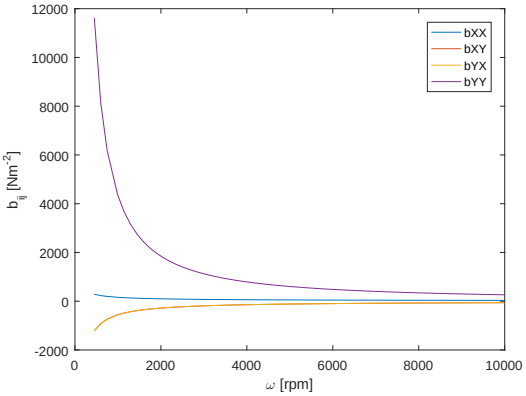

Fig. 39: Damping coefficients

Results of this determination are displayed in fig. 38 and fig. 39. As expected, the values decrease with increasing speed of the shafts.

c) Campbell diagram and stability analysis

The Campbell diagram is created based on the modal properties of the gearbox supported by fluid bearings, with the dynamic coefficients from fig. 38 and fig. 39. The Campbell diagram is for this case depict in fig. 40 and 41. The stability analysis is created using approach in chapter 3.2.

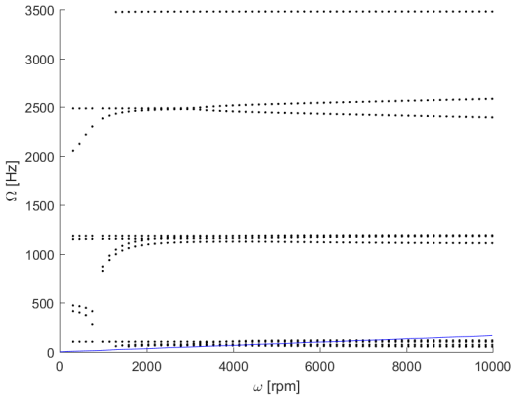

Fig. 40: Campbell diagram

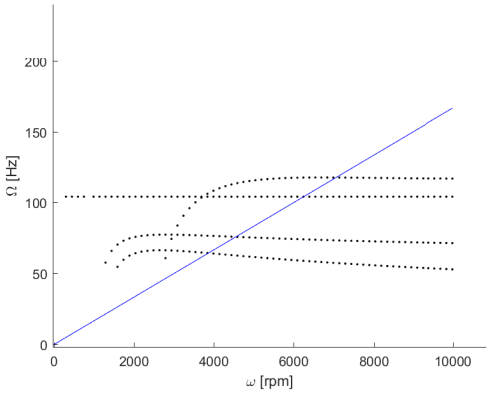

Fig. 41: Systems critical frequencies

According to the performed static analysis, we can summarize few facts. Just like the model of the single rotor in previous section, the model of the same shafts connected via gearing has also 4 very low critical frequencies. The model of the gearbox is also stable for all angular velocities within the proposed range.

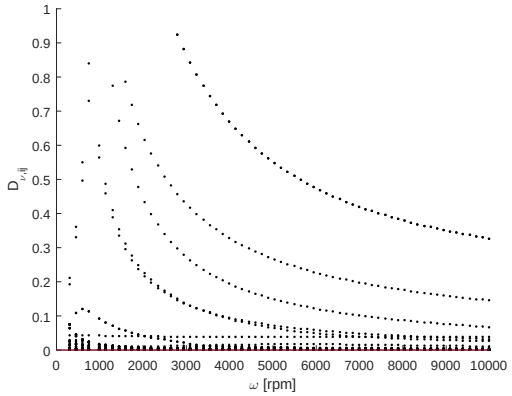

Fig. 42: Stability analysis of the rotating parts of the gearbox

Dynamic analysis

The next analysis that will be performed is a dynamic analysis. To analyze the dynamic behaviour in time domain, a computational model with reduced number of degrees of freedom is used. The reduction of the model is performed based on modal synthesis method (chapter 3.3). According to [1], the reduced model was created using first 25 eigen mode shapes which correspond to the lowest 25 eigen frequencies. The reduced model well describe the dynamic behaviour of the full model. This fact has been confirmed by numerical experiments similarly like in the model of rotor.

For this type of analysis we will use full non-linear model with kinematic transmission error and gear backslash as a excitation in gearing. The model can be expressed as (3.3.17). Parameters of the shafts and bearings are taken from chapter 4.2 and parameters of the gearing are listen in appendix. The kinematic transmission error is simulated by periodic function (2.4.6), where $\Delta^S_{z,1} = 5{\cdot}10^{-6}$ m and $\Delta^C_{z,i} = 0$ m, so only first harmonic component of the sinus function is considered. The system is excited by gear force (2.4.11).

During the dynamic simulations we will try to examine the complex dynamics of the system where both gearing and fluid film bearings nonlinear behaviour can interact. To capture the global dynamics of the system, a representative quantities have been selected. The response will be observed and analysed using vertical shaft displacement of the shafts in bearings and simultaneously the gearing deformation (2.4.1) will be analysed as well. During the dynamic simulations we will display bifurcation and waterfall diagrams of these values based on change of some operating parameter. These diagrams will be created from steady state values in time domain using numerical integration in MATLAB. For the numerical integration, the function *ode*45 will be used. We will consider the loading torque as the first significant operating parameter. We will try to examine the influence of the loading torque on the proposed values at the specific speeds of the gearbox. Based on this examination, we will try to examine the influence of the speed of the gearbox for different loading torques. Using this approach, we will be able to study the complex dynamics of this system.

1. Influence of the loading torque

For the first step, we will examine influence of the load torque, which is defined by the quantities M_1 and M_2 (see chapter above), on the dynamic behaviour of the system at a constant angular velocity of the rotor. We will choose 2 different velocities of the rotors gearbox. Based on the fact that the parameters of the shaft are exactly the same as the shaft in chapter 4.2, we can assume that the dynamic behaviour of the rotor-bearing system will be similar. This means that the oil whirl may occur at the range $\omega \in (4100, 4900)$ rpm. Based on this assumption, we will use $\omega_1 = 4500$ rpm as the first velocity and $\omega_2 = 7000$ rpm as the second reference angular velocity of the shaft that we will use for further analysis. The loading torque is considered in range $M \in (10, 500)$ Nm. Results of the analysis are displayed below. Summary of the results is in the end of this chapter.

a) Dynamic analysis at angular velocity of the gearbox $\omega = 4500$ rpm

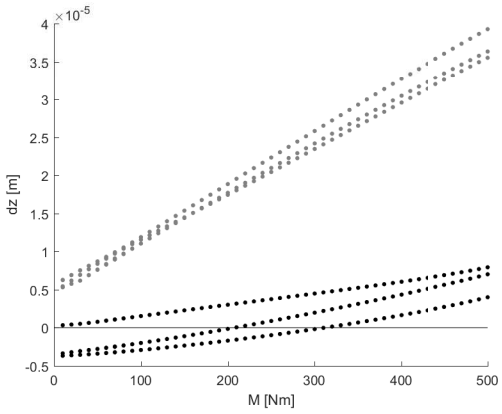

Fig. 43: Bifurcation diagram of gearing deformation based on increasing torque

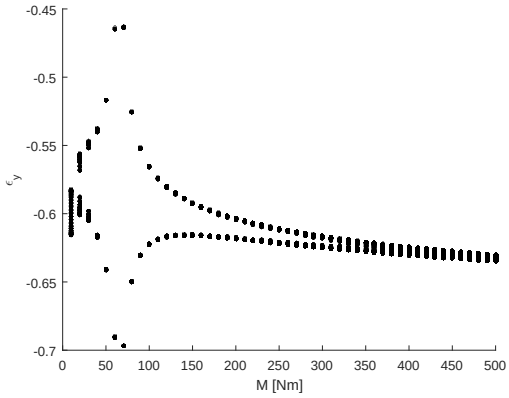

Fig. 44: Bifurcation diagram of ϵ_y of bearing B_1

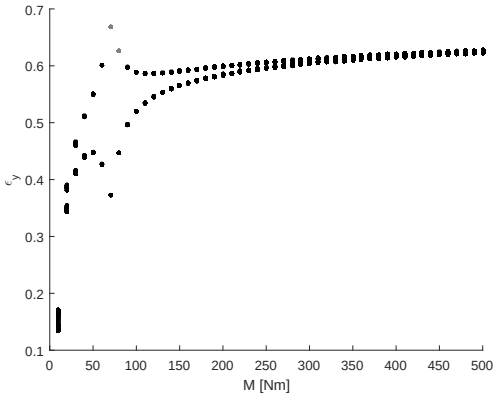

Fig. 45: Bifurcation diagram of ϵ_y of bearing B_3

b) Dynamic analysis at angular velocity of the gearbox $\omega = 7000$ rpm

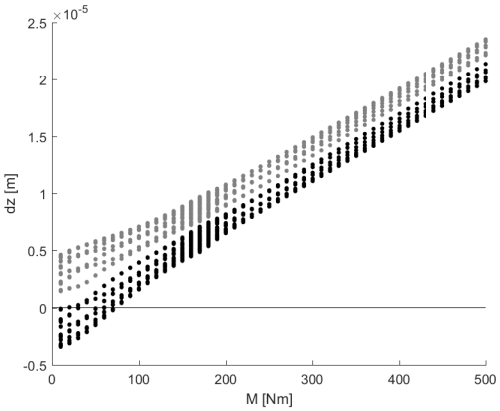

Fig. 46: Bifurcation diagram of gearing deformation

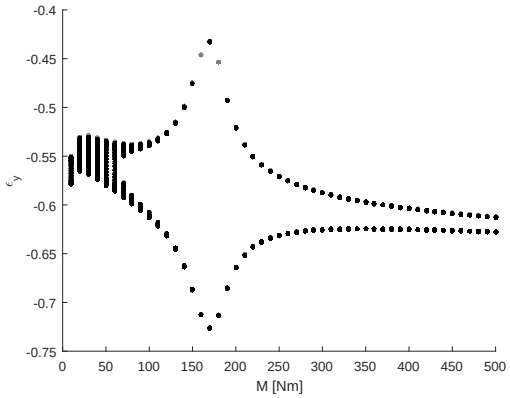

Fig. 47: Bifurcation diagram of ϵ_y of bearing B_1

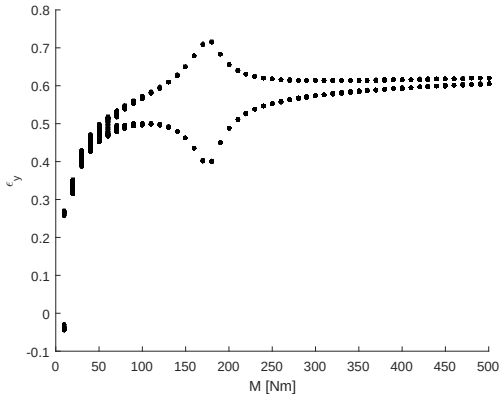

Fig. 48: Bifurcation diagram of ϵ_y of bearing B_3

In the figs. 43 - 45, there is the influence of the increasing torque M on the gearing deformation and vertical displacements of the rotor in bearings B_1 and B_3 for constant angular velocity $\omega = 4500$ rpm. It is important to mention that if the value of the gearing deformation is negative, it means that the mating teeth loss contact between them and the gears vibrate within the clearance. According to the given results, we can say that with the increasing torque, values of the gearing deformation are also increasing. You can see that the gears lost the contact within the range $M \in (10, 320)$ Nm. From the fig. 44 and fig. 45, you can see that for $M = 70$ Nm there is a resonance due to the non-linear forces in bearings. With increasing torque, the amplitudes of the values decreased for constant speed.

If it comes to higher velocity of the rotor ($\omega = 7000$ rpm), the results are depict in fig. 46 - fig. 48. Unlike for the previous velocity, the gears have lost the contact within lower range of loading torque $M \in (10, 70)$ Nm. On the other hand, the resonance of the bearings vertical displacements occurred in this case as well but, with the change of the velocity, the resonance peak moved to higher values of the torque.

According to the proposed analysis we can summarize a few points related to the influence of the loading torque.

- Lower loading torque may lead to intermittent loss of contact between the teeth in gearing. This condition causes vibration in the gearing and may create noise that can spread through the whole gearbox, it can also cause a wear of the gearing.
- The loading torque has influence on the dynamic behaviour of the shaft in bearings as well. With increasing torque, the amplitudes of the shaft displacements within bearings are decreasing and the vibration within the bearing is being suppressed. This fact may have a significant influence on the bearing stability that we will be examined in the next part.

2. Influence of the increasing speed of the gearbox

For the second analysis, we will be examining influence of the increasing velocity of the shafts on the dynamic behaviour of the gearbox at constant loading torque. Based on the previous analysis, we will choose 3 different configurations of the loading torque. Firstly, the unloaded system will be examined ((a) M=0 Nm), where the oil whirl may occur. Then we select the torque at which the contact for oil whirl frequency was lost ((b) M=100 Nm) and a torque without loss of gear contact ((b) M=500 Nm). Results for all loading torque configurations are displayed below.

a) Influence of the gearbox speed on unloaded system → M=0 Nm

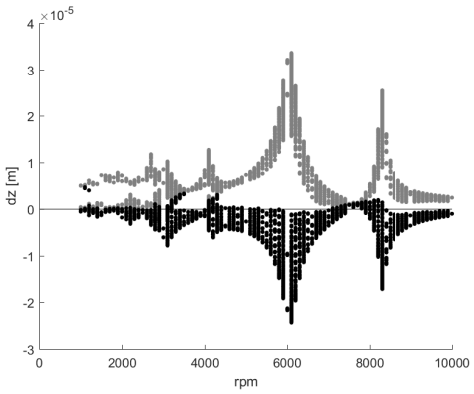

Fig. 49: Bifurcation diagram of gearing deformation based on angular velocity of shafts

The results of this analysis of the unloaded system are displayed in the fig. 49 - fig. 53. From the fig. 49, we can say that for the unloaded system, the gears lost the contact of the mating teeth within whole proposed range of the speed of the shafts. We can see resonance peaks which correspond with the harmonic and sub-harmonic critical frequencies due to the harmonic excitation provided by kinematic transmission error and unbalance force. The peaks n_p [rpm] correspond to critical frequencies Ω_c which can be expressed as

$$\Omega_c = \frac{n_p}{60} p_z \quad [Hz], \tag{4.3.1}$$

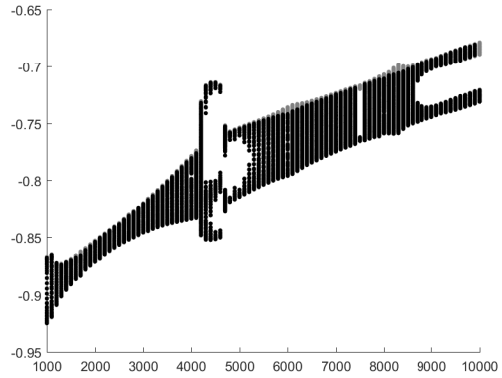

Fig. 50: Bifurcation diagram of ϵ_y of bearing B_1 based on angular velocity of the shaft

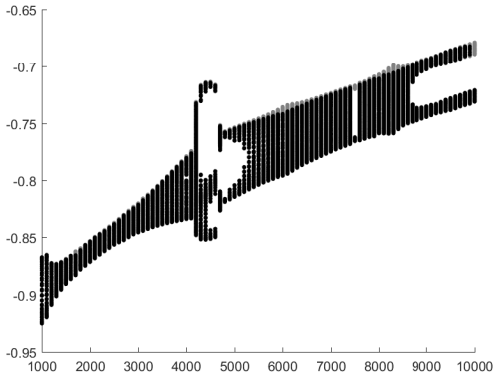

Fig. 51: Bifurcation diagram of ϵ_y of bearing B_3 based on angular velocity of the shaft

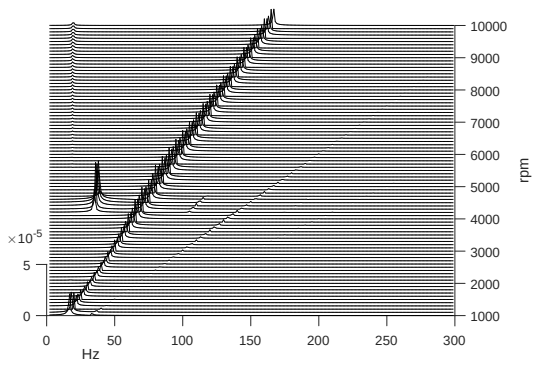

Fig. 52: Waterfall diagram of ϵ_y based on angular velocity of the shaft

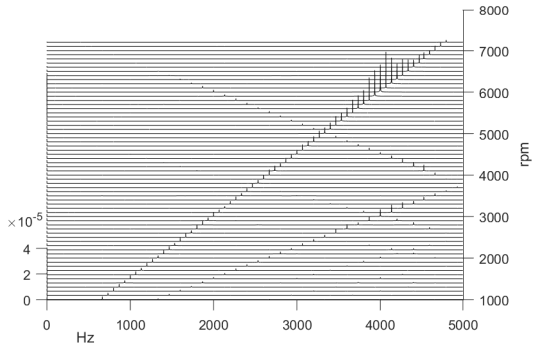

Fig. 53: Waterfall diagram of d_z based on angular velocity of the shaft

where p_z is the number of teeth. For example, the peak at $n_p = 6100$ [rpm] corresponds to first critical frequency $\Omega_c = 3900$ [Hz] (see fig. 41). The peak at $n_p = 8300$ [rpm] corresponds to the 2n critical frequency. Other peaks correspond to sub-harmonic critical frequencies due to the harmonic excitation. In the fig. 53 there is a waterfall diagram of the gearing deformation based on the increasing velocity of the shafts. In this diagram, the speed frequency of the rotor multiplied by number of teeth ($1x p_z$) and its sub-harmonic doubled value occurred. This diagram is depict for speed of the gearbox within range $\omega \in (1000, 7200)$ [rpm], because for higher velocities, higher frequencies occur in the signal and according to the signal sampling frequency, the Nyquist sampling theorem [32] is no longer valid .

As expected, oil whirl occurred at $\omega \in (4100, 4900)$ rpm. This condition can be seen from fig. 50 - fig. 52.

If we want to analyse the influence between the dynamic behaviour of gearing and the vibrating of the rotor within bearings, we can see that the oil-whirl instability did not have a significant recognisable impact on the gearing deformation. On the other hand, the frequencies located in resonance peaks of the gearing deformation increased amplitudes of the vibrating rotor within bearings. This behaviour may be observed at $\omega = 6100$ rpm and $\omega = 8200$ rpm, but the vibrations are not destructive for the system.

b) Influence of the gearbox speed on loaded system defined by torque M=100 Nm

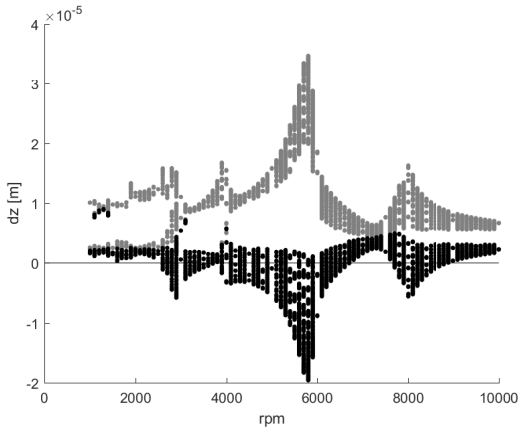

Fig. 54: Bifurcation diagram of gearing deformation

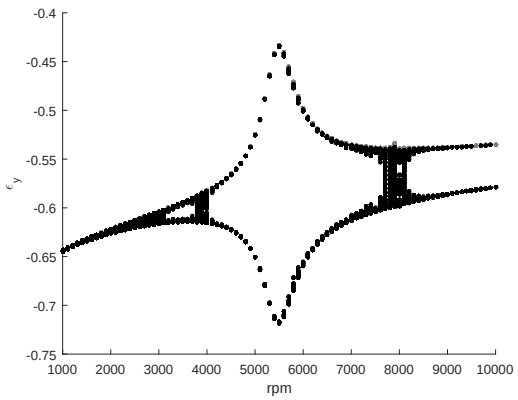

Fig. 55: Bifurcation diagram of ϵ_y of bearing B_1

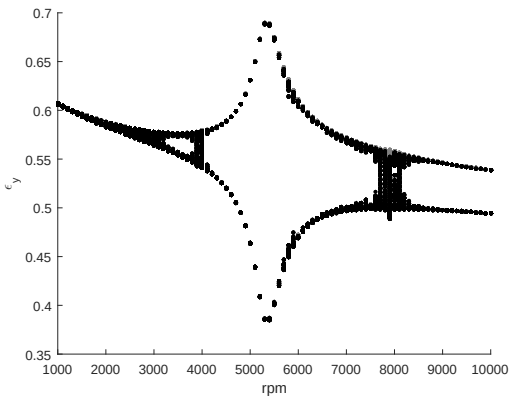

Fig. 56: Bifurcation diagram of ϵ_y of bearing B_3

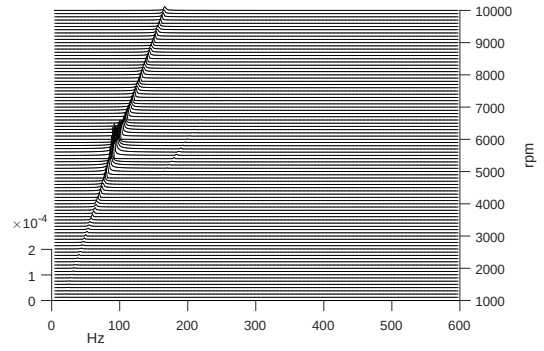

Fig. 57: Bifurcation diagram of ϵ_y of bearing B_1

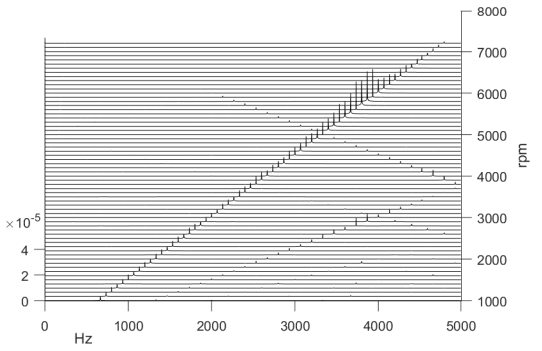

Fig. 58: Bifurcation diagram of ϵ_y of bearing B_3

The results of dynamic analysis of the loaded system defined by $M = 100$ Nm are displayed in fig. 54 - fig. 58. It is obvious, that the gearing deformation (fig. 54) for lower torque has the same trend as the deformation for unloaded system. This means, that the same resonance peaks appear in the signal, but the values increased due to the higher static deformation, this cause that the gears have not loss the contact within the whole range. For the resonance peak within $\omega = 5800$ rpm, we can see a typical shape of the curve which symbolize the jump up/jump down phenomena that can be observed in nonlinear systems [6].

If it comes to the dynamic behaviour of the rotor in bearings for loaded system, we can say that the oil whirl instability that occurred in unloaded system has been suppressed due to the loading torque caused by hydrodynamic forces. We can check whether the oil whirl has been supressed in fig. 52. This behaviour has been confirmed in [28]. This suppression is manifested by an increase of the vibration amplitudes within range $\omega \in (4100, 6800)$ rpm due to the loading torque (see fig. 44 and 47).

If we want to examine the influence of dynamic behaviour of the rotor vibrating within bearings on the gearing deformation, we can see that there is no significant impact. On the other hand, just like in the unloaded system, we can see that the vertical displacement of the rotor within bearing slightly increased at angular velocity $\omega = 3600$ rpm and $\omega = 7600$ rpm which correspond with harmonic and sub-harmonic peak of the gearing deformation. Compared to the whole range, the vibrating of the rotor within bearings for the proposed speeds manifested as a chaotic motion.

c) Influence of the gearbox speed on loaded system defined by torque M=500 Nm

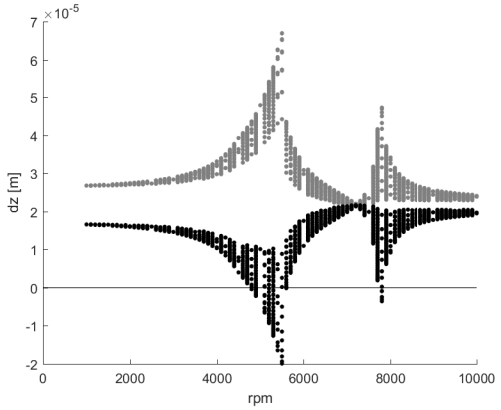

Fig. 59: Bifurcation diagram of gearing deformation

The results of dynamic analysis of the loaded system defined by $M = 500$ Nm are displayed in fig. 59 - fig. 63. For this configuration, the values of the gearing deformation (fig. 59) increased due to the higher static deformation. Interesting fact is that the sub-harmonic resonance peaks have been suppressed due to the higher loading torque. Only harmonic frequencies corresponding to the 1. and 2. critical frequencies remained in the signal. The gears lost the contact within the range of resonance peaks, so within $\omega \in (4800, 5700)$ rpm and $\omega \in (7800, 8900)$ rpm.

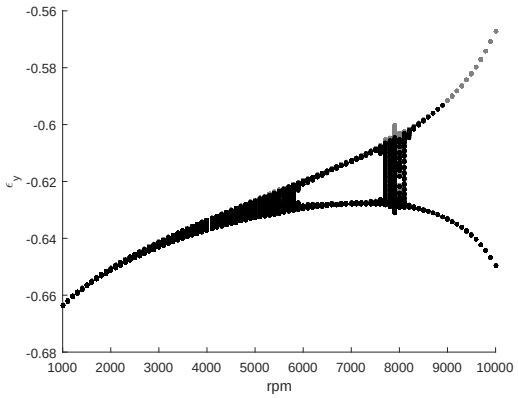

Fig. 60: Bifurcation diagram of ϵ_y of bearing B_1

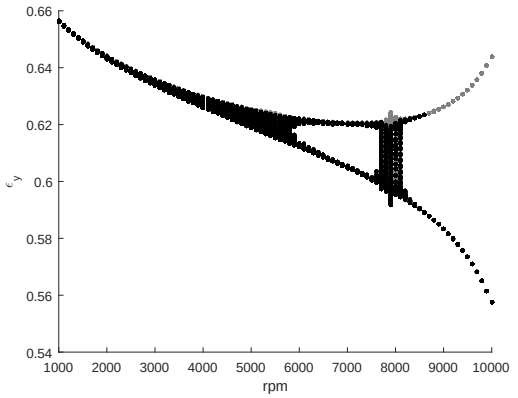

Fig. 61: Bifurcation diagram of ϵ_y of bearing B_3

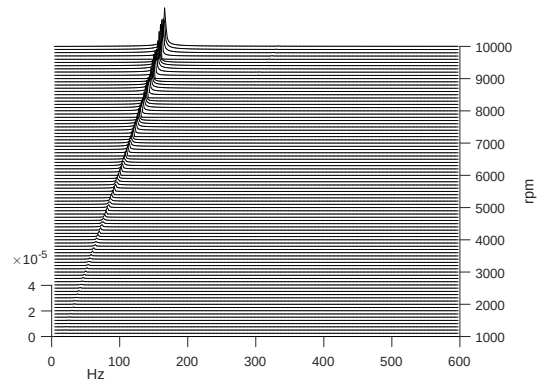

Fig. 62: Bifurcation diagram of ϵ_y of bearing B_1

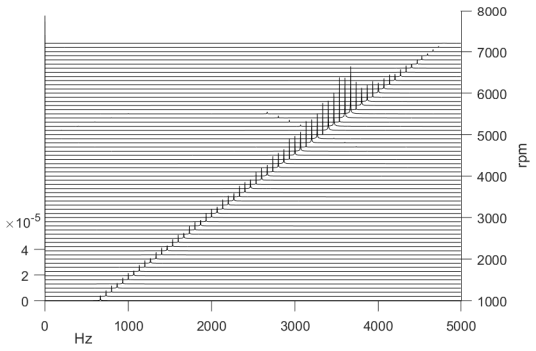

Fig. 63: Bifurcation diagram of ϵ_y of bearing B_3

The oil whirl instability has been suppressed again, but due to the higher loading torque the resonance peak moved to the higher frequency (see the influence of the loading torque fig. 44 and 47).

In terms of dynamic interaction between gearing and rotor vibrating within bearing, again, we can see that the vertical displacement of the rotor within bearing slightly increased and act as a chaotic motion at angular velocity $\omega = 7600$ rpm which correspond the peak in gearing deformation.

Summary

According to the performed dynamic analyses we can summarize a few observations. In terms of the influence of the loading torque on the dynamic behaviour of the gearing, we can definitely say, that low loading torques may cause loss of contact of mating teeth in gearing (fig. 43). On the other hand for high loads, the sub-harmonic resonance frequencies are suppressed and they are not excited (fig. 59). The loading torque has also impact on the static deformation of the gearing.

If we want to analyse the influence of the loading torque on the dynamic behaviour of the rotor vibrating within bearing clearance, we can say, that with increasing torque the oil whirl instability is being suppressed (fig. 55, fig. 60) and due to the nonlinear hydrodynamic forces, the amplitudes and the resonance peaks of the bearings rotor displacements are moving to the higher frequency zones (fig. 44, fig. 47, fig. 55 and fig. 60).

In terms of an interaction between dynamic behaviour of the gearing and dynamics of bearings, we can say, that vibrating of the rotor within bearings does not have a significant impact on the gearing deformation. On the other hand internal excitation of the gearing caused by kinematic transmission error has slight influence on the behaviour of the rotor in bearings. This fact was shown for example in fig. 49 and fig. 50. To be sure of this effect, we can perform dynamic analysis of this system without a unbalance force of the discs, so without the main source of oil whirl instability, so we can see the pure influence of the internal gear excitation on the bearings behaviour. This analysis was performed and the results are depict in fig. 64.

In the fig. 64, there is a detail of the gearing deformation resonance peaks and vertical displacement of the rotor within bearing depending on the speed within range $\omega \in (5000, 10000)$ rpm for the model without unbalance force. It has been confirmed that the oil whirl frequency has not appeared. Rectangles define the area of the resonance peaks of gearing deformation and corresponding area of the value ϵ_y. It is obvious that there is a slight influence of the dynamic behaviour of the gearing on the vibrating of the rotor within bearings.

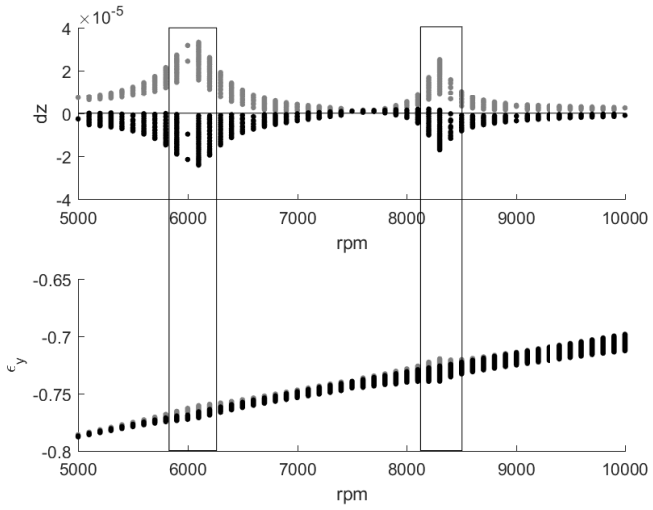

Fig. 64: Detail of the influence of the gearing internal excitation on the vertical displacement of the shaft within bearing

5 Conclusion

This diploma thesis dealt with modelling and dynamic analysis of rotating systems supported by fluid bearings. The thesis mainly focused on examining the non-linear phenomena in this non-linear dynamic systems.

Rotating systems can be divided into subsystems like shafts, bearing or gearing. The chapter 2 dealt with modelling of these subsystems using finite element method. The methodology of modelling of shaft was presented. Then the thesis focused on mathematical models of fluid bearings, where the most important part is expression of hydrodynamic forces acting on the shaft rotating within bearing clearance. With linear approximation of the hydrodynamic forces, we can get approximation of stiffness and damping coefficients depending on the shaft velocity. In the chapter 2.4, the mathematical model of gearing was introduced. The gearing force may include non-linear forces caused by gear backslash, time-varying meshing stiffness or kinematic transmission error which is the main source of internal excitation in gearing dynamics.

The chapter 3 aimed at approaches that we can use for dynamic analysis of rotating systems. These approaches may include state space model, numerical integration, modal analysis and modal synthesis method. Using modal analysis, we can create Campbell diagram to see systems critical frequencies or to perform stability analysis. In case of fluid film bearings dynamics, waterfall diagram is a important part of examining dynamic behaviour of these systems. With waterfall diagram we can determine whether the oil whirl or oil whip instability is excited. Modal synthesis method which is used for creating reduced mathematical models was presented. In the end of the chapter, typical non-linear phenomena of the rotating systems were summarized.

In the application part of the thesis, three applications of the proposed methods and analyses were created. According to the mathematical models, computational models for all three applications were developed in computational system MATLAB. Computational models were used for examination of typical non-linear phenomena in rotating systems.

The biggest emphasis was put on dynamic analysis of the single stage gearbox, where the interaction between gearing and bearing couplings were examined. According to the results, we can summary the following observations:

- Low loading torque may lead to intermittent loss of contact of mating teeth in gearing. Oil whirl instability can occur with lightly loaded gearboxes supported by fluid bearings.
- High loading torque suppress sub-harmonic frequencies and increase static deformation of the gearing. The loading torque have also influence on the dynamic behaviour of the gearboxes with fluid bearings. High loading torques can suppress instability of type oil whirl and the system can become stable.
- Vibrating of the rotor at whirl frequency does not have a significant impact on the gearing vibration (deformation).
- Internal excitation of the gearing caused by kinematic transmission error has a slight influence on the behaviour of the rotor in bearings, but these oscillations are not destructible.

Further work

A possible extension of the diploma thesis could consist in the use of more accurate models. In the case of gearing model, in [2] there is a model of gearing that consider the width of the gears, so the contact is not only at one point. In the case of fluid bearings, hydrodynamic forces obtained by numerical solution of the Reynolds equation may be included.

If it comes to the application part, it would be interesting to further examine the dynamic behaviour of the gearbox under operating conditions and experimentally validate the created computational model, especially in resonant areas.

References

[1] M.Byrtus, Kmitání převodových ústrojí se silnými nelinearitami ve vazbách, Fakulta aplikovaných věd v Plzni, 2006.

[2] M. Byrtus, M. Hajžman, V. Zeman, Dynamika rotujících soustav, Vydavatelství ZČU v Plzni, 2010.

[3] Š. Dyk, J. Rendl, M. Byrtus, L. Smolík, Dynamic coefficients and stability analysis of finite-length journal bearings considering approximate analytical solutions of the Reynolds equation, Tribology international, 2018.

[4] L. Smolík, Modelování kmitání a dynamická analýza rotorů turbodmychadel, disertační práce, Fakutla aplikovaných věd v Plzni, 2018.

[5] J. Zapoměl, Počítačové modelování příčného kmitání rotorů uložených v hydrodynamických ložiskách a squeeze filmových tlumičích. Ostrava: VŠB - Technická univerzita Ostrava, 2007. ISBN 978-80-248-1593-0.

[6] V. Zeman, J. Slavík, V.Stejskal , Základy dynamiky strojů, Vydavatelství ČVUT v Praze, 1997.

[7] J. Zhan, M. Fard, R. Jazar, A CAD-FEM-QSA integration technique for determining the time-varying meshing stiffness of gear pairs, Measurement, 2016.

[8] Yamamoto, T. Ishida, Y.: Linear and Nonlinear Rotordy-dnamics (A Modern Treatment with Applications). John Wiley & Sons, Inc., New York, 2001.

[9] Gasch, R. Nordman, R. Pfützner, H.: Rotordynamik. 2. Auflage. Springer-Verlag, Berlin, Heidelberg, New York, 2002.

[10] Driot, N. Rigaud, E. Sabot, J. Perret-Liaudet, J.: Prediction ofgearbox noise variability from tolerances on profile and helix angle. In Proceedings of The 29th International Congress and Exhibition on Noise Control Engineering. Nice,2000, France.

[11] Zeman, V. Dupal, J. Hlaváč, Z. Kovář, L. Voldřich, J.: Vibration analysis of the car gearbox. Engineering mechanics 2001, ÚTAM AV CR,Praha 2001.

[12] Šimek, J., 2008. Kluzná ložiska a uložení rotorů [online]. Praha: Techlab [cit. 2018-06-20]. Available from: http:/ www.techlab.cz/cs/loziska.html

[13] Ngyen-Schafer, H., 2012. Rotordynamics of Automotive Turbochargers: Linear and Nonlinear Rotordynamics, Bearing Design, Rotor Balancing. Berlin: Springer. ISBN 978-3-642-27517-3.

[14] Schweizer, B., 2009. Oil whirl, oil whip and whirl/whip synchronization occurring in rotor systems with full-floating ring bearings. Nonlinear Dyn. 57(4), 509-532.

[15] Tian, L., W. J.Wang and Z. J. PENG, 2012. Effects of bearing outer clearance on the dynamic behaviours of the full- floating ring bearing supported turbocharger rotor. Mech Syst Signal Pr. 31, 155-175.

[16] Zhang, H., Z. Shi, F. Gi a A. Ball, 2011. Modelling of outer and inner film oil pressure for floating ring bearing clearance in turbochargers. J Phys Conf Ser. 305: 12-21.

[17] San Andrés, L. a J. Kerth, 2004. Thermal effects on the performance of floating ring bearings for turbochargers. P I Mech Eng J-J Eng. 218: 437-450.

[18] Novotný, P., P. Škara a J. Hliník, 2018. The effective computational model of the hydrodynamics journal floating ring bearing for simulations of long transient regimes of turbocharger rotor dynamics. Int J Mech Sci. 148, 611-619.

[19] A. Kahraman, R. Singh, Non-linear dynamics of a spur gear pair, J. Sound Vib. (1990), https://doi.org/10.1016/0022-460X(90)90582-K.

[20] G.W. Blankenship, A. Kahraman, Steady state forced response of a mechanical oscillator with combined parametric excitation and clearance type nonlinearity, J. Sound Vib. 185 (1995) 743e765.

[21] A. Kahraman, G.W. Blankenship, Experiments on nonlinear dynamic behavior of an oscillator with clearance and periodically time-varying parameters, J. Appl. Mech. 64 (1997) 217, https://doi.org/10.1115/1.2787276.

[22] A. Raghothama, S. Narayanan, Bifurcation and chaos in geared rotor bearing system by incremental harmonic balance method, J. Sound Vib. (1999), https://doi.org/10.1006/jsvi.1999.2264.

[23] Y. Yang, L. Cao, H. Li, Y. Dai, Nonlinear dynamic response of a spur gear pair based on the modeling of periodic mesh stiffness and static transmission error, Appl. Math. Model. 72 (2019) 444e469, https://doi.org/10.1016/j.apm.2019.03.026.

[24] H. Motahar, F.S. Samani, M. Molaie, Nonlinear vibration of the bevel gear with teeth profile modification, Nonlinear Dynam. 83 (2016) 1875e1884, https://doi.org/10.1007/s11071-015-2452-z.

[25] J. Yang, T. Lim, Dynamics of coupled nonlinear hypoid gear mesh and time-varying bearing stiffness systems, SAE Int. J. Passeng. Cars - Mech. Syst. 4 (2011) 1039e1049, https://doi.org/10.4271/2011-01-1548.

[26] J. Wang, T.C. Lim, Effect of tooth mesh stiffness asymmetric nonlinearity for drive and coast sides on hypoid gear dynamics, J. Sound Vib. 319 (2009) 885e903, https://doi.org/10.1016/j.jsv.2008.06.021.

[27] S. Natsiavas Theodossiades, Non-linear dynamics of gear-pair systems with periodic stiffness and backlash, J. Sound Vib. (2000), https://doi.org/10. 1006/jsvi.1999.2490.

[28] S. Theodossiades, S. Natsiavas, On geared rotordynamic systems with oil journal bearings, J. Sound Vib. 243 (2001) 721e745, https://doi.org/10.1006/ jsvi.2000.3430.

[29] S. Baguet, G. Jacquenot, Nonlinear couplings in a gear-shaft-bearing system, Mech. Mach. Theor. 45 (2010) 1777e1796, https://doi.org/10.1016/j. mechmachtheory 2010.08.009.

[30] Z. Liu, Z. Liu, J. Zhao, G. Zhang, Study on interactions between tooth backlash and journal bearing clearance nonlinearity in spur gear pair system, Mech. Mach. Theor. 107 (2017) 229e245, https://doi.org/10.1016/j.mechmachtheory.2016.09.024.

[31] D. Shin, A. Palazzolo, Nonlinear analysis of a geared rotor system supported by fluid film journal bearings, Journal of Sound and Vibration, Volume 475, 2020, 115269, ISSN 0022-460X. https://doi.org/10.1016/j.jsv.2020.115269.

[32] Levesque, Luc. (2014). Nyquist sampling theorem: Understanding the illusion of a spinning wheel captured with a video camera. Physics Education. 49. 697. 10.1088/0031-9120/49/6/697.

[33] J. Rendl, Výpočtové modelování kluzných ložisek pro úlohy dynamiky rotorů, diplomová práce, Fakulta aplikovaných věd v Plzni, 2017.

Appendix

1. Parameters of the gearing

gearing stiffness	k_z [10^8 Nm^{-1}]	4
gearing damping	b_z [Nms^{-1}]	1600
kinematic transmission error	Δ_z [10^{-6} m]	5
gearing module	m [mm]	4
number of teeth	p_z [-]	40
pressure angel	α [°]	20
helix angel	β [°]	0
deflection angle	γ [°]	0
discs diameter	r [mm]	80
discs indentation	a,b [mm]	0

Tab. 7: Parameters of the gearing for single stage gearbox